Journal of Building Engineering 69 (2023) 106318

Contents lists available at ScienceDirect

Journal of Building Engineering

journal homepage: www.elsevier.com/locate/jobe

Full length article

Multi-layered slab 1D conduction heat transfer for buildings discrete event simulations

Víctor Manuel Soto Francés *, José Manuel Pinazo Ojer, Emilio José Sarabia Escrivá

Departamento de Termodinámica Aplicada, ETSII, Edificio 5J, C/Camino de Vera S/N. Universitat Politècnica de València, València, 46022, Comunitat Valenciana, Spain

ARTICLE INFO

Keywords:
Conduction heat transfer function
1*D* conduction heat transfer
Laplace
Successive state transition
Multi-layered slab

ABSTRACT

The 1*D* conduction heat transfer in multi-layered slabs is fundamental to building energy simulation. Its solution could be split into two big categories: finite difference and root-finding methods. These latter are also known as Laplace or Conduction heat Transfer Function methods (CTF).

The paper briefly reviews why none of them, in its current formulation, fits the new trend based on event-driven simulation. It proposes a new CTF whose inputs are the conduction heat fluxes $\dot{q}$ and the responses are the superficial temperature speeds $\dot{T}$ on both slab sides. Thus it could be classified as a root-finding procedure. However, it employs a solution rooted in the uncommon *Successive State Transition* (SST) method from the 80's Japanese school. Moreover, it proves that both superficial temperatures T can also be solved using this SST method. The outcome is a solution procedure with many advantages; the main one is that it does suit the novel event-driven paradigm.

Finally, the paper illustrates the procedure with an example.

1. Introduction

A fundamental problem that any building energy simulation solves is the 1*D* conduction heat transfer through each layer of a wall or slab, modeled by the well-known partial differential equation:

$$\frac{\partial^2 T}{\partial x^2} = \frac{1}{\alpha}\frac{\partial T}{\partial t} \tag{1}$$

Between each layer, there is no thermal contact resistance, i.e., the touching points of two layers share the same temperature, and there is continuity of the conduction heat flux $\dot{q}$.

Traditionally, the strategies to simulate or estimate the energy response of a multi-layered slab, according to the previous model, might be split into two big categories:

- Finite difference
- Conduction (heat) transfer functions (CTF)

The first is usually represented graphically using an electrical analogy that the literature renames RC, i.e., resistance and capacitance models. See Fig. 1.

* Corresponding author.
E-mail addresses: vsoto@ter.upv.es (V.M. Soto Francés), jmpinazo@ter.upv.es (J.M. Pinazo Ojer), emsaes@upvnet.upv.es (E.J. Sarabia Escrivá).

https://doi.org/10.1016/j.jobe.2023.106318
Received 1 December 2022; Received in revised form 3 March 2023; Accepted 14 March 2023
Available online 16 March 2023
2352-7102/© 2023 The Author(s). Published by Elsevier Ltd. This is an open access article under the CC BY license (http://creativecommons.org/licenses/by/4.0/).

Symbols

α	Thermal diffusivity $k/\rho c_p$ [m^2/s]
Δt	Elapsed time or time step [s]
$\dot{q}$	Conduction heat flux [W/m^2]
$\mathcal{G}(s)$	Transfer function
$\mathcal{L}f$	Laplace Transform of f
ϕ_S	Time response of signal S to an input impulse
A_k^m	Residue at a pole k of $\mathcal{G}^m(s)$
C	Thermal capacity [J/m^{2}K]
m	Index $\in \{00, 01, 10, 11\}$ to identify output–input signals, respectively
Q	Energy [J/m^2]
R	Thermal resistance [m^{2}K/W]
s	Complex Laplace variable
T	Temperature [K]

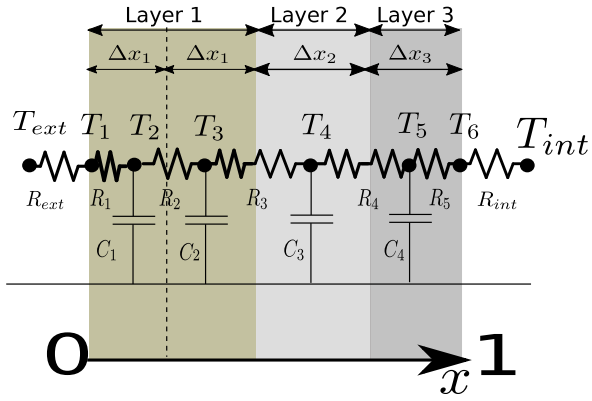

Fig. 1. Scheme of a discrete multi-layered slab model, with lumped masses and thermal resistances. RC-model.

The second is also known as *root finding methods* since they employ the Laplace Transform $\mathcal{L}$. In Ref. [1], the reader may find a comparison between them.

Mitalas and Stephenson, in an ASHRAE report [2] dated in 1971, proposed the conduction heat transfer functions $\mathcal{G}^m(s)$ shown in Eq. (2) (see also [3]).

$$\begin{bmatrix} \mathcal{L}\dot{q}_0 \\ \mathcal{L}\dot{q}_1 \end{bmatrix} = \begin{bmatrix} \mathcal{G}^{00}(s) & \mathcal{G}^{01}(s) \\ \mathcal{G}^{10}(s) & \mathcal{G}^{11}(s) \end{bmatrix} \cdot \begin{bmatrix} \mathcal{L}T_0 \\ \mathcal{L}T_1 \end{bmatrix} \tag{2}$$

They relate the Laplace Transform of the conduction heat transfer $\dot{q}$ at each side (denoted by 0 and 1) of the multi-layered slab with the Laplace Transform of the superficial temperatures on both sides. The first and second superscripts of $\mathcal{G}^{ab}(s)$ indicate the $\dot{q}_a$ response and T_b excitation sides, respectively. *Notice that the wall is "excited" by the superficial temperatures on both sides*. Years passed and fifty years later, Morrison's book [4] (2020) still describes Mitalas' method as state of the art.

Conventionally, the current simulation engines choose the time step as; fixed, variable, adaptive, or some intermediate strategy among the previous ones. In any case, time always drives the simulation. However, the recent trend [5] moves to a flexible event-driven (and not time-driven) paradigm. The aim is to devise a general-purpose event-driven simulator that separates the model definition from their solution. During the calculation, each component schedules when it will suffer an internal state transition with the final goal of spending more computation time on those fast-evolving elements. The procedure focuses on the state of system components, not the flow of time. Wetter et al. [6] greatly favor this new paradigm. Unfortunately, they claim that the traditional solution to some fundamental problems needs to work better within the events paradigm. One of them is, precisely, the conventional solution of $1D$ multi-layered conduction heat transfer posed at the beginning. As a temporary bypass solution, they propose to co-simulate [7].

To the previous difficulties, De Wilde [8] adds up what has been called *the building energy performance gap*, also supported by many others (see for instance [9,10]). De Wilde points out, among other causes, the "*mismatch between first principle energy models*".

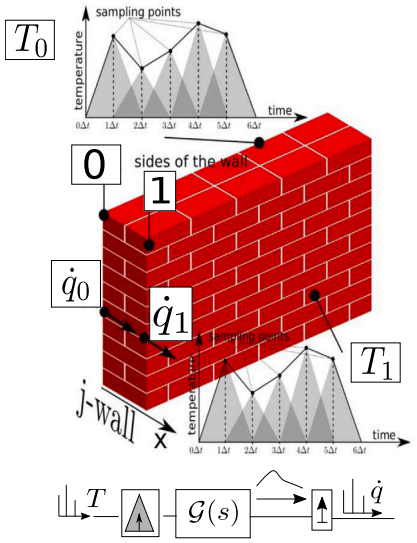

Fig. 2. Conventional Mitalas' method. *Source:* Adapted from our previous paper [12].

2. Drawbacks of traditional methods

The paper's aim is not to discuss the previous problems in detail. However, this section gathers the main drawbacks of the traditional methods that the paper tries to address.

In finite difference approach, a finite number of degrees of freedom replaces the original problem. Livio et al. in [11] showed how to improve the RC model employed by the ISO 52016 – 1 standard. The ISO proposes a wall model with five degrees of freedom and a fixed hourly time step. Livio et al. [11] modified this "oversimplified" model. They proposed a variable amount of wall states (nodes) and a shorter time-step $\Delta t = 15$ [min], because particularly Italy has many monumental and heavy-construction old buildings. That paper stated that one must cautiously choose the amount and location of the nodes (capacities) of the RC model according to the time step and the physical properties of the layers. The higher the sampling time–frequency (i.e., shorter time steps), the greater the amount of nodes. Once the number of nodes is determined, the computation should track their states throughout the simulation. At first sight, it could fit the event-driven paradigm. Nevertheless, if the wall sampling frequency differs from the one for which the RC model was created, then the model loses its accuracy. Therefore is not a good option in practice.

In the case of the CTF, Fig. 2 illustrates the traditional solution applied to Eq. (2). The input signals are the superficial temperatures on both sides, T_0 and T_1, sampled at a fixed predefined rate. These impulse trains are obviously not "physical" and thus cannot be fed directly into the wall CTF, i.e., the $\mathcal{G}^m(s)$. The method uses a holder or shaping element for these impulses. One may think of *any* "sensible" holder shape. Traditionally, the shape is triangular. The idea behind this selection is to form a continuous piecewise-linear temperature signal. Since the heat conduction model is a linear equation, the sum of triangles delayed by a time step (i.e., convolution) creates such a "sensible" temperature profile. After using this *artificially*-shaped piece-wise linear input-signal T, although the output-signal $\dot{q}$ is continuous, the same fixed sampling rate is used at the output (see Fig. 2). The result is an input–output signal relationship at a predetermined sampling rate Δt. Livio et al. in [1], showed that this procedure is quicker than the RC-model for $\Delta t = 1$ [h] but similar for $\Delta t = 15$ [min].

It is evident that this method does not fit an event-driven simulation. Moreover, the conduction heat flux evolution, which allows such *imposed* linear temperature profiles, cannot be tracked. This leads to other problems (see more details in [12]). The transient response of a superficial temperature to a sudden change of heat input is exponential-like rather than linear. Therefore, to get a good approximation of heat loads and comfort, a $\Delta t = 15$ [min] or lower is usually recommended in the guidebooks.

Recently, [13] studied the use of the conventional Mitalas' CFTs (see Eq. (2)) in an event-driven simulation. It already employed a formulation based on the *Successive State Transition method* (SST for short) with these *traditional* CTFs. The SST method belongs to the Japanese school in the $80's$ (see [14]), but unfortunately, it has been overlooked for a long. Paper [13] exploited, among others, its capability to allow a variable time step. Unexpectedly, its conclusions were negative: the problems associated with imposing a superficial temperature hinder the expected advantages of a full event-driven simulation. As aforementioned, the details can be found in the previous work [12], nevertheless it is noteworthy to describe *some of its ideas already published there*. Assume the boundary wall of a room in thermal equilibrium with it at 22 [°C]. Suddenly, the wall receives a radiation heat-source; $\dot{q}_{rad-src} = 10\,[\mathrm{W/m^2}]$ for 2 [h], that is, an energy input rate of 36000 $[\mathrm{J/hm^2}]$ during 2 [h], and afterwards this source is switched off. Fig. 3 shows the superficial temperature profile on the side where the radiation source is applied. The two profiles correspond to two different time steps: 5 [min]

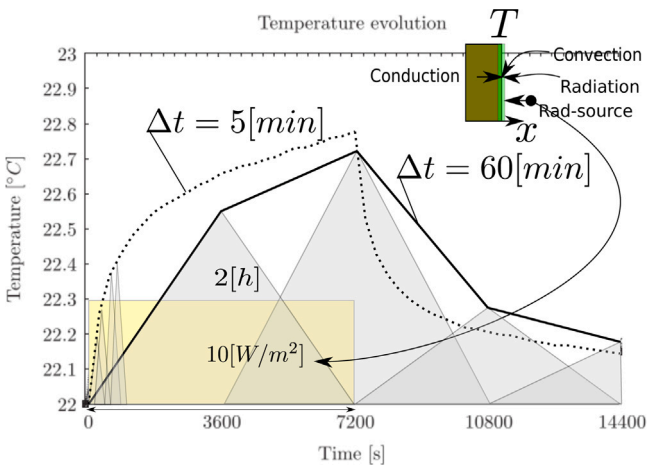

Fig. 3. Mitalas' method applied to a simple case, with $\Delta t = 5$ [min] and $\Delta t = 60$ [min].
Source: Adapted from our previous paper [12].

and 60 [min], using the Mitalas' method (remark: the sampling rates and holders are displayed for comparison). Obviously, the first profile is closer to the actual temperature response than the second, as it has the correct exponential-like profile. The small sketch at the top-right part of Fig. 3 shows the well-known heat power balance on the surface. It just says that the sum of all the ingoing heat fluxes into the surface must be zero at any instant, i.e., formally:

$$\dot{q}_{conduction}(t) + \dot{q}_{convection}(t) + \dot{q}_{radiation}(t) + \dot{q}_{src}(t) = 0 = \dot{q}_{storage}(t) \tag{3}$$

Recall that the Mitalas' method only forces Eq. (3) at the sampling points, along with the linear temperature profiles between them. Nevertheless, imagine placing meters on that surface (see details in [12]) for any energy type. The meters sum should always give zero, i.e., the integral of Eq. (3) over time until an instant t' should fulfill:

$$\int_0^{t'} \left(\dot{q}_{conduction}(t) + \dot{q}_{convection}(t) + \dot{q}_{radiation}(t) + \dot{q}_{src}(t)\right) dt = 0 = \int_0^{t'} \dot{q}_{storage}(t) dt \tag{4a}$$

$$\text{SUM}(t') = Q_{cond}(t') + Q_{conv}(t') + Q_{rad}(t') + Q_{src}(t') = 0 = Q_{storage}(t') \tag{4b}$$

Fig. 4, based on data from Table 6 of [12], shows that this condition breaks down for "common" simulation time steps, like $\Delta t = 60$ [min] (see the $Q_{storage}$ curve). The smaller the time step, the smaller this energy unbalance. Fortunately, this cancels over time. This outcome has the following interpretation. For big Δt Mitalas' method overlooks that the temperature response may be exponential-like. Fig. 3 shows that, in this case, the actual temperature should rise quickly, but it does it slowly. Therefore after the first hour, Fig. 4 marks $Q_{storage}(1\,[\text{h}]) > 0$, while, as expected, the individual meters are negative because the energy flows out from the surface, which is being heated. But their sum is unbalanced. In other words, it is like some missing energy is being diverted to storage. After switching off the radiation source, the opposite occurs. The actual temperature decreases quickly, but the Mitalas' method assumes a slow descent. Now from $t = 3$ [h] on, $Q_{storage} < 0$, i.e., the previously (and falsely) stored energy comes back, keeping the temperature artificially high (see Fig. 3). The net result is that, from the room's point of view, the method adds an extra heat capacity to the walls, which is related to selecting a big time-step Δt.

It is clear that the superficial temperature determines the wall heat exchange with its surroundings which in turn modifies the incoming heat flux to the wall and vice versa. So, there is a feedback loop. To correctly track this process-loop behavior, the superficial temperature velocity $\dot{T}$ must be known. A high $\dot{T}$ value means that the wall state is changing fast, and thus alongside, it ought to force a reevaluation (sampling event) of the heat flux $\dot{q}$.

The new CTF became a necessary solution based on previous works and [13]. So, the event-driven simulation paradigm should give up using the *traditional* CTF for $1D$ conduction heat transfer. The paper analyzes a novel proposal, along with a solution based on the SST method. Its main features are:

- Fits event-driven simulations.
- It can be designed to cope with the shortest *expected* time-step.
- The computational cost is self-adaptive. A shorter time between events requires a higher computation load and vice versa.
- The slab is excited by conduction heat fluxes, thus allowing tracking of the energy flows and the thermal disequilibrium processes.

Finally, before the conclusions section, some examples illustrate the method.

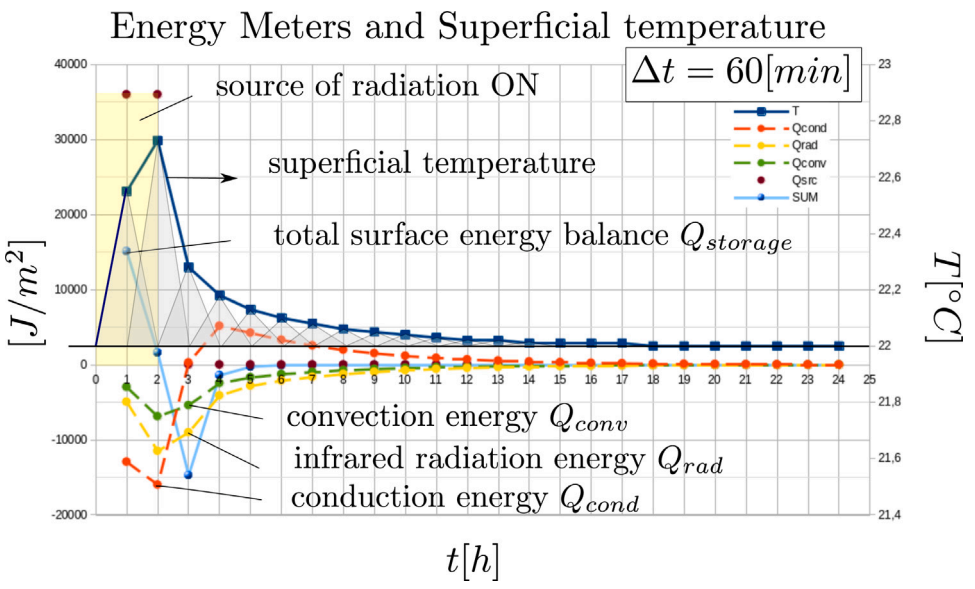

Fig. 4. Energy unbalance through the surface of Fig. 3 due to the time step $\Delta t = 60\,[\text{min}]$ employed in the Mitalas' method. *Source:* Adapted from our previous paper [12].

3. Theory

3.1. The new conduction heat transfer functions $\mathcal{G}''(s)$

The goal is to solve the following new Eq. (5):

$$\begin{bmatrix} \mathcal{L}\dot{T}_0 \\ \mathcal{L}\dot{T}_1 \end{bmatrix} = \begin{bmatrix} \mathcal{G}''^{,00}(s) & \mathcal{G}''^{,01}(s) \\ \mathcal{G}''^{,10}(s) & \mathcal{G}''^{,11}(s) \end{bmatrix} \cdot \begin{bmatrix} \mathcal{L}\dot{q}_0 \\ \mathcal{L}\dot{q}_1 \end{bmatrix} \tag{5}$$

By comparing Eq. (2) (conventional CTF) and (5) (new CTF), it shows up that the input and output signals are different. Now the slab response is driven by the conduction heat flux $\dot{q}$ applied on both sides. Notice also that the response is not the superficial temperature but its time derivative, rate of change $\dot{T}$, or simply its velocity.

Let us deduce the new $\mathcal{G}''^{,m}(s)$. Appendix A exposes the deduction of the traditional CTF. In order to get Eqs. (5), (A.8) must be inverted:

$$\begin{bmatrix} \mathcal{L}T_0 \\ \mathcal{L}T_1 \end{bmatrix} = \begin{bmatrix} \mathcal{G}'^{00}(s) & \mathcal{G}'^{01}(s) \\ \mathcal{G}'^{10}(s) & \mathcal{G}'^{11}(s) \end{bmatrix} \cdot \begin{bmatrix} \mathcal{L}\dot{q}_0 \\ \mathcal{L}\dot{q}_1 \end{bmatrix} \tag{6}$$

where:

$$\mathcal{G}'^{,00}(s) = \frac{-AA \cdot BB}{(1 - AA \cdot DD)} \tag{7a}$$

$$\mathcal{G}'^{,10}(s) = \frac{-BB}{(1 - AA \cdot DD)} = -\mathcal{G}'^{,01}(s) \tag{7b}$$

$$\mathcal{G}'^{,11}(s) = \frac{BB \cdot DD}{(1 - AA \cdot DD)} \tag{7c}$$

Notice the prime over $\mathcal{G}'^{,m}(s)$. Since the time derivative is required, by multiplying by s:

$$\mathcal{G}''^{,00}(s) = \frac{-s \cdot AA \cdot BB}{(1 - AA \cdot DD)} = s \cdot \mathcal{G}'^{,00}(s) \tag{8a}$$

$$\mathcal{G}''^{,10}(s) = \frac{-s \cdot BB}{(1 - AA \cdot DD)} = -\mathcal{G}''^{,01}(s) = s \cdot \mathcal{G}'^{,10}(s) \tag{8b}$$

$$\mathcal{G}''^{,11}(s) = \frac{s \cdot BB \cdot DD}{(1 - AA \cdot DD)} = s \cdot \mathcal{G}'^{,11}(s) \tag{8c}$$

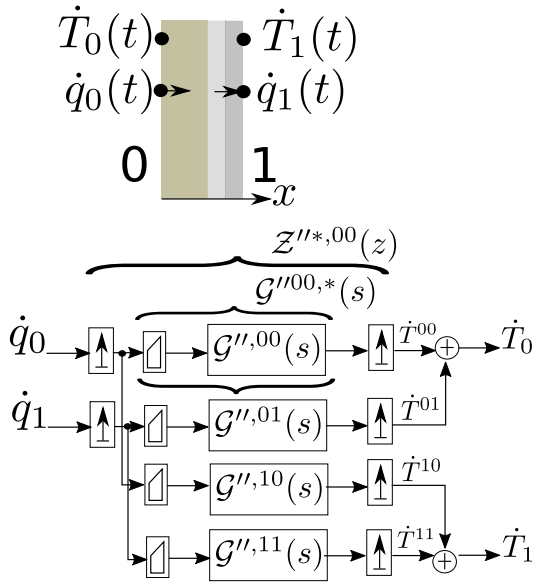

Fig. 5. Successive state transition (STT) scheme applied to the new CTF. The heat fluxes $\dot{q}$ are inputs, and the temperature velocities $\dot{T}$ are outputs.

All previous $\mathcal{G}'^{,m}(s)$ and $\mathcal{G}''^{,m}(s)$ in general have the form:

$$\mathcal{G}'^{,m}(s) = \frac{H'^{,m}(s)}{G'^{,m}(s)} \tag{9}$$

(Remark:the numerator of $\mathcal{G}''^{,m}(s)$ is just $H''^{,m}(s) = sH'^{,m}(s)$, but $G''^{,m}(s) = G'^{,m}(s)$). Thus, the *residue* theorem of complex variable theory is applied to obtain the reverse Laplace transform. This theorem leads to the following expression for each matrix element in Eq. (6):

$$\mathcal{L}(\phi_T^m(t)) = G'^m(s) = \frac{A_0^m}{s} + \sum_{k=1}^{\infty} \frac{A_k^m}{s+\alpha_k} \tag{10}$$

or directly in its time form:

$$\phi_T^m(t) = A_0^m + \sum_{k=1}^{\infty} A_k^m \cdot e^{-\alpha_k \cdot t} \tag{11}$$

Here, by A_k^m, it is meant the residue at pole $-\alpha_k$. The exponent $m \in \{00, 01, 10, 11\}$ indicates which $\mathcal{G}'^{,m}(s)$ are implied. The poles are the points s_k on the complex plane where $\mathcal{G}'^{,m}(s)$ goes to infinity. All these poles can be found on the negative real axis. Therefore by α_k let us denote its absolute value. The infinite set of poles and residues uniquely identify the thermal response of the multi-layered slab. Looking at Eq. (11) or (10), it can be deduced that 0 is also a simple pole of $\mathcal{G}'^{,m}(s)$.

As aforementioned, the Laplace transform property:

$$\mathcal{L}(\phi_{dT/dt}^m(t)) = s \cdot \mathcal{L}(\phi_T^m(t)) - \overbrace{T(0)}^{=0} \tag{12}$$

allow us to finally get the target transfer function:

$$G''^{,m}(s) = s \cdot G'^{,m}(s) = A_0^m + \sum_{k=1}^{\infty} \frac{A_k^m \cdot s}{s+\alpha_k} \tag{13}$$

which shares residues and poles (but the zero) with $\mathcal{G}'^{,m}(s)$, but has another form.

3.2. The successive state transition formulation

Fig. 5 illustrates the idea behind the SST method. Briefly, the methodology consists of the following steps. First, the method needs an abrupt end in the holder. Thus a trapezoid suffices. The result is a trapezoid-pulse of conduction heat flux during Δt. Next, the product of the Laplace transform of this holder by $\mathcal{G}''^{,m}(s)$ is renamed $\mathcal{G}''^{,m,*}(s)$. Finally, it samples the input heat fluxes and output temperature velocities at the end of Δt. This corresponds to computing the $\mathcal{Z}$ transform of $\mathcal{G}''^{,m,*}(s)$. Conversely to conventional

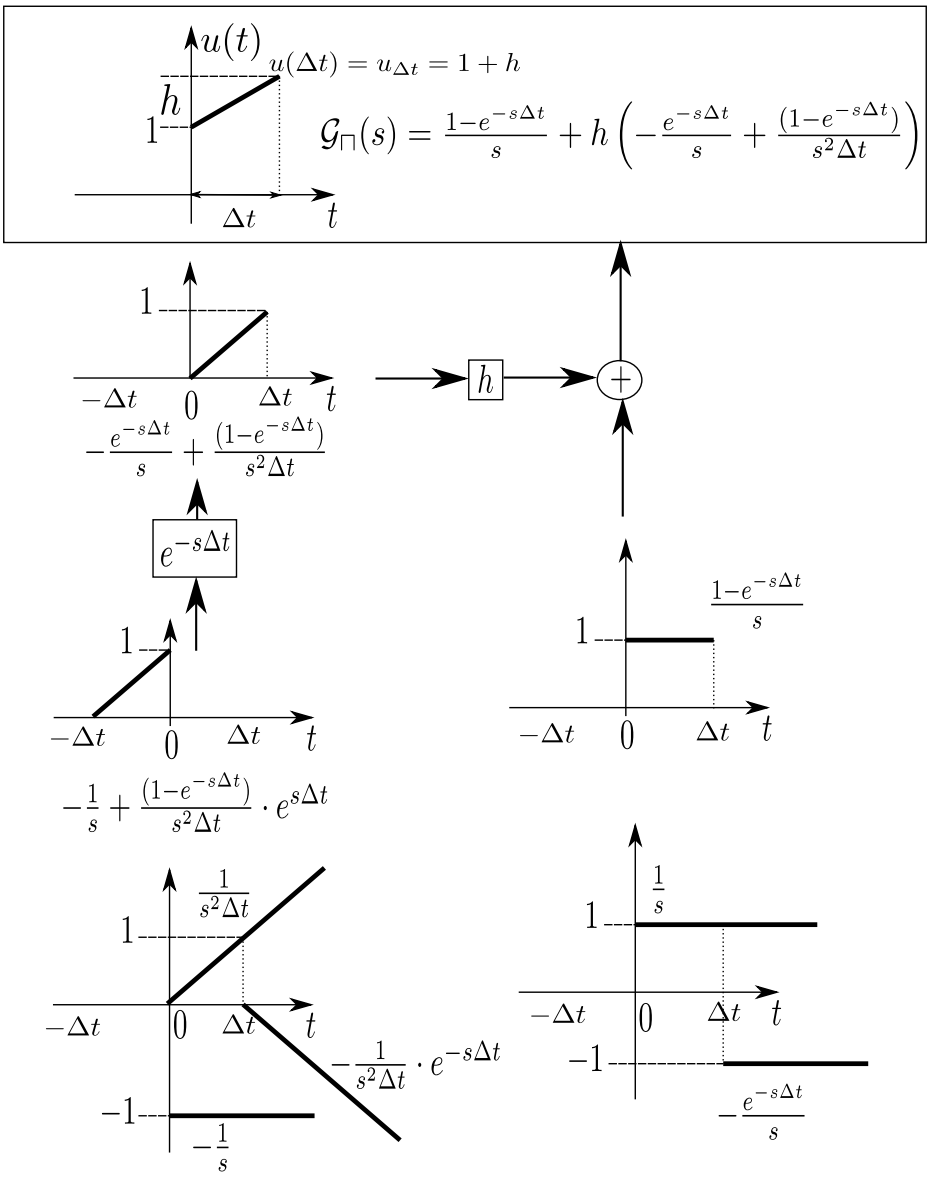

Fig. 6. Laplace transform of the trapezoidal holder.

methods, it does not require keeping the sampling frequency fixed. Only the first input–output values are related in the $\mathcal{Z}$-transform (i.e., the coefficients of the term z^{-1}). After the time-lapse Δt, the slab *internal states* are stored. They will be necessary to construct the subsequent response to the next incoming heat flux pulse. In other words, the method transports the slab state over time, after each input. This transport allows computing the output superficial temperature velocities after a beforehand unknown Δt.

The mathematical details are as follows.

Fig. 6 describes how to obtain the Laplace transform of the trapezoid holder. It is parametrized by: Δt the duration of the heat pulse, and $h \cdot u_0 = u_{\Delta t} - u_0$, where $u_{t'} = u(t'), t' = t_n - t_{n-1}$. When the pulse is unitary, i.e. $u_0 = 1$ then $h = u_{\Delta t} - 1$ or $u_{\Delta t} = 1 + h$. In our case, the input-signal $u \equiv \dot{q}$ is the conduction heat flux on either slab side.

By using Eq. (13), the $\mathcal{G}'^{,m,*}(s)$ expression is:

$$\begin{aligned} &\mathcal{G}''^{,m,*}(s) = \mathcal{G}'^{,m}(s) \cdot \mathcal{G}_{\sqcap}(s) \\ &\mathcal{G}''^{,m,*}(s) = A_0^m \cdot \mathcal{G}_{\sqcap}(s) + \sum_{k=1}^{\infty} \frac{A_k^m}{(s+\alpha_k)} \left[(1 - e^{-s\Delta t}) + h \left(-e^{-s\Delta t} + \frac{(1 - e^{-s\Delta t})}{s\Delta t} \right) \right] \end{aligned} \tag{14}$$

The next step is computing the $\mathcal{Z}$-transform of the Eq. (14).

$$\mathcal{Z}(\mathcal{G}'^{,m,*}(s)) = A_0^m \cdot \mathcal{Z}(\mathcal{G}_\Pi(s)) + \sum_{k=1}^{\infty} \mathcal{Z}(f_k^m(s)) \tag{15}$$

where $f_k^m(s)$ represents each k-term inside the summation symbol in Eq. (14). The following general relationships between Laplace-transform and $\mathcal{Z}$-transform have been employed:

$$\mathcal{Z}\left[\frac{Be^{\mp s\Delta t}}{s+a}\right] = \frac{Bz^{\mp n}}{1-e^{-a\Delta t}z^{-1}} \tag{16a}$$

$$\mathcal{Z}\left[\frac{Be^{\mp s\Delta t}}{s(s+a)}\right] = \frac{1}{a}\cdot\frac{B(1-e^{-a\Delta t})z^{(-1\mp n)}}{(1-z^{-1})(1-e^{-a\Delta t}z^{-1})} \tag{16b}$$

$$\mathcal{Z}\left[\frac{Be^{\mp ns\Delta t}}{s^2}\right] = \frac{B\Delta t z^{(-1\mp n)}}{(1-z^{-1})^2} \tag{16c}$$

The $\mathcal{Z}$-transform of $\mathcal{G}_\Pi(s)$ is:

$$\mathcal{Z}(\mathcal{G}_\Pi(s)) = \frac{1}{(1-z^{-1})} - \frac{z^{-1}}{(1-z^{-1})} + h\left(-\frac{z^{-1}}{(1-z^{-1})} + \frac{z^{-1}}{(1-z^{-1})^2} - \frac{z^{-2}}{(1-z^{-1})^2}\right) = 1 \tag{17}$$

while the $\mathcal{Z}$-transform of each term $f_k^m(s)$ is given by:

$$\begin{aligned}\mathcal{Z}(f_k(s)) &= \frac{A_k^m(1-z^{-1})}{(1-e^{-\alpha_k\Delta t}z^{-1})} + \\ &A_k^m h\left[\frac{-z^{-1}}{(1-e^{-\alpha_k\Delta t}z^{-1})} + \frac{(1-e^{-\alpha_k\Delta t})z^{-1}}{\alpha_k\Delta t(1-z^{-1})(1-e^{-\alpha_k\Delta t}z^{-1})} - \frac{(1-e^{-\alpha_k\Delta t})z^{-2}}{\alpha_k\Delta t(1-z^{-1})(1-e^{-\alpha_k\Delta t}z^{-1})}\right]\end{aligned} \tag{18}$$

operating, in the previous expression, on the term between square brackets:

$$\begin{aligned}\mathcal{Z}(f_k(s)) &= \frac{A_k^m(1-z^{-1})}{(1-e^{-\alpha_k\Delta t}z^{-1})} + \\ &A_k^m h\left[\frac{-\alpha_k\Delta t(1-z^{-1})z^{-1} + (1-e^{-\alpha_k\Delta t})z^{-1} - (1-e^{-\alpha_k\Delta t})z^{-2}}{\alpha_k\Delta t(1-z^{-1})(1-e^{-\alpha_k\Delta t}z^{-1})}\right] = \\ &= \frac{A_k^m(1-z^{-1})}{(1-e^{-\alpha_k\Delta t}z^{-1})} + A_k^m h\left[\frac{-\alpha_k\Delta t(1-z^{-1})z^{-1} + (1-e^{-\alpha_k\Delta t})(z^{-1}-z^{-2})}{\alpha_k\Delta t(1-z^{-1})(1-e^{-\alpha_k\Delta t}z^{-1})}\right] = \\ &= \frac{A_k^m(1-z^{-1})}{(1-e^{-\alpha_k\Delta t}z^{-1})} + A_k^m h\left[\frac{(1-e^{-\alpha_k\Delta t}-\alpha_k\Delta t)z^{-1}}{\alpha_k\Delta t(1-e^{-\alpha_k\Delta t}z^{-1})}\right]\end{aligned} \tag{19}$$

Let us name U^* (here $U^* = \dot{q}^*$) and V^* (here $V^* = \dot{T}^*$), the sampled input and output signals, respectively. To simplify the notation using Eq. (15):

$$V^*(z) = \mathcal{Z}(\mathcal{G}'^{,m,*}(s))(z)\cdot U^*(z) = A_0^m \cdot \overbrace{\mathcal{Z}(\mathcal{G}_\Pi(s))}^{=1}\cdot U^*(z) + \sum_{k=1}^{\infty}\mathcal{Z}(f_k^m(s))\cdot U^*(z) \tag{20}$$

The sampled output and input signals have the following form in $\mathcal{Z}$-transform form, respectively:

$$\begin{aligned}V^*(z) &= v_0 + v_1\cdot z^{-1} + v_2\cdot z^{-2} + \cdots \\ U^*(z) &= u_0 + u_1\cdot z^{-1} + u_2\cdot z^{-2} + \cdots\end{aligned} \tag{21}$$

The coefficients of equal z power in Eq. (20) must equated. As aforementioned, the z^{-1} coefficient is the goal. The first term on the right-hand side of the Eq. (20) contributes to this coefficient with:

$$A_0^m \cdot u_1 \cdot z^{-1} \tag{22}$$

Now labeling $W_k^m(z)$ to the result of each term of the summation in Eq. (20):

$$\begin{aligned}W_k^m(z) &= \mathcal{Z}(f_k^m(s))\cdot U^*(z) = \\ &= \frac{A_k^m(1-z^{-1})}{(1-e^{-\alpha_k\Delta t}z^{-1})}\cdot U^*(z) + A_k^m h\left[\frac{(1-e^{-\alpha_k\Delta t}-\alpha_k\Delta t)z^{-1}}{\alpha_k\Delta t(1-e^{-\alpha_k\Delta t}z^{-1})}\right]\cdot U^*(z)\end{aligned} \tag{23}$$

by clearing:

$$W_k^m(z)\cdot(1-e^{-\alpha_k\Delta t}z^{-1}) = A_k^m(1-z^{-1})\cdot U^*(z) + A_k^m h\left[\frac{(1-e^{-\alpha_k\Delta t}-\alpha_k\Delta t)z^{-1}}{\alpha_k\Delta t}\right]\cdot U^*(z) \tag{24}$$

the left-hand side is:

$$\begin{aligned} &w_{k,0}^m + w_{k,1}^m\cdot z^{-1} + w_{k,2}^m\cdot z^{-2} + \cdots + \\ &-w_{k,0}^m e^{-\alpha_k\Delta t}\cdot z^{-1} - w_{k,1}^m e^{-\alpha_k\Delta t}\cdot z^{-2} + w_{k,2}^m\cdot z^{-2} - \cdots = \end{aligned} \tag{25}$$

or:

$$w_{k,0}^m + (w_{k,1}^m - w_{k,0}^m e^{-\alpha_k\Delta t})\cdot z^{-1} + \cdots \tag{26}$$

The expansion, on the right-hand side of Eq. (24) is:

$$\begin{aligned} &A_k^m\cdot u_0 + A_k^m\cdot u_1\cdot z^{-1} + \cdots + \\ &\quad -A_k^m\cdot u_0\cdot z^{-1} - A_k^m\cdot u_1\cdot z^{-2} - \cdots + \\ &A_k^m h u_0\frac{(1-e^{-\alpha_k\Delta t}-\alpha_k\Delta t)}{\alpha_k\Delta t}\cdot z^{-1} + \cdots \end{aligned} \tag{27}$$

Equating the coefficients of z^{-1} in Eq. (24):

$$w_{k,1}^m - w_{k,0}^m e^{-\alpha_k\Delta t} = A_k^m(u_1-u_0) + A_k^m\cdot h u_0\cdot\frac{(1-e^{-\alpha_k\Delta t}-\alpha_k\Delta t)}{\alpha_k\Delta t} \tag{28}$$

But as $hu_0 = u_1 - u_0$:

$$w_{k,1}^m - w_{k,0}^m e^{-\alpha_k\Delta t} = A_k^m(u_1-u_0) + A_k^m\cdot(u_1-u_0)\cdot\frac{(1-e^{-\alpha_k\Delta t}-\alpha_k\Delta t)}{\alpha_k\Delta t} \tag{29}$$

the next expression is obtained:

$$w_{k,1}^m - w_{k,0}^m\cdot e^{-\alpha_k\Delta t} = A_k^m\frac{(1-e^{-\alpha_k\Delta t})}{\alpha_k\Delta t}\cdot(u_1-u_0) \tag{30}$$

or:

$$w_{k,1}^m = w_{k,0}^m\cdot e^{-\alpha_k\Delta t} + A_k^m\frac{(1-e^{-\alpha_k\Delta t})}{\alpha_k\Delta t}\cdot(u_1-u_0) \tag{31}$$

This last is the successive state transition equation for the transfer function m. It relates the relaxation of a *sub-system state* (or mode), indexed by k and corresponding to pole $-\alpha_k$, between two successive sampling points. Building up the output response at the end of Δt (i.e., in z^{-1}) leads to:

$$v_1 = A_0^m\cdot u_1 + \sum_{k=1}^{\infty} w_{k,1}^m \tag{32}$$

Finally, it remains to reconstruct the signals as appear in Fig. 5. The current state is renamed $0 \equiv (n-1)$ and the new one, after Δt, $1 \equiv n$. The correct labels for the input and output signals are, respectively: $v \equiv \dot{T}$ and $u \equiv \dot{q}$. The output temperature rate at each side is the sum of the two output contributions due to the conduction heat flux pulses at both sides. As a result, the linear expressions of the superficial velocities on both sides as a function of the new conduction heat fluxes, are:

$$\dot{T}_{0,n} = A_0^{00}\cdot\dot{q}_{0,n} + \sum_{k=1}^{\infty} w_{k,n}^{00} + A_0^{01}\cdot\dot{q}_{1,n} + \sum_{k=1}^{\infty} w_{k,n}^{01} = A_0^{00}\cdot\dot{q}_{0,n} + A_0^{01}\cdot\dot{q}_{1,n} + \sum_{k=1}^{\infty} w_{k,n}^{0} \tag{33a}$$

$$\dot{T}_{1,n} = A_0^{10}\cdot\dot{q}_{0,n} + \sum_{k=1}^{\infty} w_{k,n}^{10} + A_0^{11}\cdot\dot{q}_{1,n} + \sum_{k=1}^{\infty} w_{k,n}^{11} = A_0^{10}\cdot\dot{q}_{0,n} + A_0^{11}\cdot\dot{q}_{1,n} + \sum_{k=1}^{\infty} w_{k,n}^{1} \tag{33b}$$

Eq. (33) define the total state of 0-side w_k^0, as the sum of the states 00 and 01. In concrete, at n: $w_{k,n}^0 = w_{k,n}^{00} + w_{k,n}^{01}$. Analogously, on the other side $w_{k,n}^1 = w_{k,n}^{10} + w_{kn}^{11}$. Using the explicit expressions (31) the *successive state transition* at both sides is just:

$$\begin{aligned} w_{k,n}^0 =& w_{k,(n-1)}^0\cdot e^{-\alpha_k\Delta t} + \\ &A_k^{00}\frac{(1-e^{-\alpha_k\Delta t})}{\alpha_k\Delta t}\dot{q}_{0,n} + A_k^{01}\frac{(1-e^{-\alpha_k\Delta t})}{\alpha_k\Delta t}\dot{q}_{1,n} + \\ &-A_k^{00}\frac{(1-e^{-\alpha_k\Delta t})}{\alpha_k\Delta t}\dot{q}_{0,(n-1)} - A_k^{01}\frac{(1-e^{-\alpha_k\Delta t})}{\alpha_k\Delta t}\dot{q}_{1,(n-1)} \end{aligned} \tag{34}$$

$$\begin{aligned} w^1_{k,n} =& w^1_{k,(n-1)} \cdot e^{-\alpha_k \Delta t} + \\ & A^{10}_k \frac{(1-e^{-\alpha_k \Delta t})}{\alpha_k \Delta t} \dot{q}_{0,n} + A^{11}_k \frac{(1-e^{-\alpha_k \Delta t})}{\alpha_k \Delta t} \dot{q}_{1,n} + \\ & -A^{10}_k \frac{(1-e^{-\alpha_k \Delta t})}{\alpha_k \Delta t} \dot{q}_{0,(n-1)} - A^{11}_k \frac{(1-e^{-\alpha_k \Delta t})}{\alpha_k \Delta t} \dot{q}_{1,(n-1)} \end{aligned} \tag{35}$$

In short, Eq. (33) can be written more simply:

$$\dot{T}_{0,n} = a^{00} \cdot \dot{q}_{0,n} + a^{01} \cdot \dot{q}_{1,n} + d^0 \tag{36a}$$

$$\dot{T}_{1,n} = a^{10} \cdot \dot{q}_{0,n} + a^{11} \cdot \dot{q}_{1,n} + d^1 \tag{36b}$$

where by defining two secondary transition parameters:

$$\varphi_k = e^{-\alpha_k \Delta t} \tag{37a}$$

$$r_k = \frac{(1-\varphi_k)}{\alpha_k \Delta t} \tag{37b}$$

, the coefficients are:

$$a^m = A^m_0 + \sum_{k=1}^{\infty} r_k \cdot A^m_k \tag{38a}$$

$$d^0 = \sum_{k=1}^{\infty} w^0_{k,(n-1)} \cdot \varphi_k - \left(\sum_{k=1}^{\infty} r_k \cdot A^{00}_k \right) \cdot \dot{q}_{0,(n-1)} - \left(\sum_{k=1}^{\infty} r_k \cdot A^{01}_k \right) \cdot \dot{q}_{1,(n-1)} \tag{38b}$$

$$d^1 = \sum_{k=1}^{\infty} w^1_{k,(n-1)} \cdot \varphi_k - \left(\sum_{k=1}^{\infty} r_k \cdot A^{10}_k \right) \cdot \dot{q}_{0,(n-1)} - \left(\sum_{k=1}^{\infty} r_k \cdot A^{11}_k \right) \cdot \dot{q}_{1,(n-1)} \tag{38c}$$

and the *successive state transition* expressions, i.e., Eqs, (34) and (35) are:

$$w^0_{k,n} = w^0_{k,(n-1)} \cdot \varphi_k + r_k \left(A^{00}_k \dot{q}_{0,n} + A^{01}_k \dot{q}_{1,n} \right) - r_k \left(A^{00}_k \dot{q}_{0,(n-1)} + A^{01}_k \dot{q}_{1,(n-1)} \right) \tag{39}$$

$$w^1_{k,n} = w^1_{k,(n-1)} \cdot \varphi_k + r_k \left(A^{10}_k \dot{q}_{0,n} + A^{11}_k \dot{q}_{1,n} \right) - r_k \left(A^{10}_k \dot{q}_{0,(n-1)} + A^{11}_k \dot{q}_{1,(n-1)} \right) \tag{40}$$

So, summarizing, Eq. (36) represent the outputs $\dot{T}_{0,n}$, $\dot{T}_{1,n}$ due to the linear evolution, from their previous values, of the new conduction heat fluxes $\dot{q}_{0,n}$, $\dot{q}_{1,n}$, at the end of Δt.

Notice that the response computation relies on the internal states, indexed by k, on which the $\{a^m\}$ and $\{d^0, d^1\}$ depend. The independent terms $\{d^0, d^1\}$, are functions of the previous states $(w^0_{k,(n-1)}, w^1_{k,(n-1)})$ and previous conduction heat fluxes $(\dot{q}_{0,(n-1)}, \dot{q}_{1,(n-1)})$ (see Eqs. (39), (40)). These $\{a^m\}$ and $\{d^0, d^1\}$ depend on the secondary parameters φ_k and r_k that take into account each internal state k and Δt.

Although the paper will discuss the implementation details afterward, it is worthwhile to point out that both (φ_k and r_k) go to zero as Δt or α_k increases. Therefore, there is no need to compute an infinite series in practice.

Finally, once the response is known, at the sampling point n, the procedure must update the superficial states anew with Eqs. (39) and (40). The states must be stored as $(w^0_{k,(n-1)}, w^1_{k,(n-1)})$ to use them in the next sampling point.

3.3. SST method applied to T response

This subsection applies the SST method to the $\mathcal{G}'^{,m}(s)$ (see Eq. (10)), that relates the superficial T response with the conduction heat flux excitation. In practice, the method cannot directly compute the T response. Without going into the details, it would need an infinite series of terms. Fortunately, the $\Delta T = T_n - T_{n-1}$ does fit the SST method.

Algebraic manipulation is a bit more involved than before. Eq. (7) leads to Eq. (10) and now the $\mathcal{Z}$-transform to compute is:

$$\mathcal{Z}(G'^{,m,*}(s)) = \mathcal{Z}(G'^{,m}(s) \cdot G_{\sqcap}(s)) \tag{41}$$

Repeating those previous equations here for easy reading:

$$\mathcal{G}'^{,m}(s) = \mathcal{L}(\phi^m_T(t)) = \frac{A^m_0}{s} + \sum_{k=1}^{\infty} \frac{A^m_k}{(s+\alpha_k)}$$

$$G_{\sqcap}(s) = \frac{(1-e^{-s\Delta t})}{s} + h \cdot \left[-\frac{e^{-s\Delta t}}{s} + \frac{(1-e^{-s\Delta t})}{\Delta t s^2} \right]$$

Thus:

$$G'^{,m,*}(s) = \underbrace{A_0^m \frac{(1-e^{-s\Delta t})}{s^2}}_{I} + \underbrace{A_0^m h\left[-\frac{e^{-s\Delta t}}{s^2} + \frac{(1-e^{-s\Delta t})}{\Delta t s^3}\right]}_{II} + \sum_{k=1}^{\infty}\left[\underbrace{A_k^m \frac{(1-e^{-s\Delta t})}{s(s+\alpha_k)}}_{III} + \underbrace{A_k^m h\left[-\frac{e^{-s\Delta t}}{s(s+\alpha_k)} + \frac{(1-e^{-s\Delta t})}{\Delta t s^2(s+\alpha_k)}\right]}_{IV}\right] \tag{42}$$

where four terms are grouped, I, II, III, and IV, to facilitate their handling. The $\mathcal{Z}$-transform of each labeled term is:

$$(I) \rightarrow \quad A_0^m \frac{(1-z^{-1})\Delta t z^{-1}}{(1-z^{-1})^2} \tag{43a}$$

$$(II) \rightarrow \quad A_0^m h\left[-\frac{z^{-1}\Delta t z^{-1}}{(1-z^{-1})^2} + \frac{(1-z^{-1})\Delta t^2 z^{-1}(1+z^{-1})}{2\Delta t(1-z^{-1})^3}\right] \tag{43b}$$

$$(III) \rightarrow \quad A_k^m \frac{(1-z^{-1})(1-e^{-\alpha_k \Delta t})z^{-1}}{\alpha_k(1-z^{-1})(1-e^{-\alpha_k \Delta t}z^{-1})} \tag{43c}$$

$$(IV) \rightarrow \quad A_k^m h\left[-\frac{z^{-1}(1-e^{-\alpha_k\Delta t})z^{-1}}{\alpha_k(1-z^{-1})(1-e^{-\alpha_k\Delta t}z^{-1})} + \frac{(1-z^{-1})\left((\alpha_k\Delta t - 1 + e^{-\alpha_k\Delta t}) + (1-e^{-\alpha_k\Delta t} - \alpha_k\Delta t e^{-\alpha_k\Delta t})z^{-1}\right)z^{-1}}{\Delta t\alpha_k^2(1-z^{-1})^2(1-e^{-\alpha_k\Delta t}z^{-1})}\right] \tag{43d}$$

simplifying them:

$$(I) \rightarrow \quad A_0^m \frac{\Delta t z^{-1}}{(1-z^{-1})} \tag{44a}$$

$$(II) \rightarrow \quad A_0^m h \frac{\Delta t z^{-1}}{2(1-z^{-1})} \tag{44b}$$

$$(III) \rightarrow \quad A_k^m \frac{(1-e^{-\alpha_k\Delta t})z^{-1}}{\alpha_k(1-e^{-\alpha_k\Delta t}z^{-1})} \tag{44c}$$

$$(IV) \rightarrow \quad A_k^m h \frac{(\alpha_k\Delta t - 1 + e^{-\alpha_k\Delta t})z^{-1}}{\Delta t\alpha_k^2(1-e^{-\alpha_k\Delta t}z^{-1})} \tag{44d}$$

The general output-signal $V(z)$ to an input-signal $U(z)$ will be given by:

$$V(z) = \mathcal{Z}(G'^{,m,*}(s)) \cdot U(z) \tag{45}$$

where $V(z)$ is any superficial temperature and $U(z)$ the conduction heat flux at any side. The m determines the output–input couple, as before.

Looking at Eq. (42), $\mathcal{Z}$-transform of $[(I)+(II)]\cdot U(z)$ is the W_0^m 0-state (notice the capital W). Analogously, $[(III)+(IV)]\cdot U(z)$ is the k-state, W_k^m. Thus:

$$V(z) = \mathcal{Z}(G'^{,m,*}(s)) \cdot U(z) = W_0^m(z) + \sum_{k=1}^{\infty} W_k^m(z) \tag{46}$$

Naming the state transition W_0^m, as:

$$W_0^m(z) = W_{0,0}^m + W_{0,1}^m z^{-1} + W_{0,2}^m z^{-2} + \cdots = \\ = \left(\frac{A_0^m\Delta t z^{-1}}{(1-z^{-1})} + \frac{A_0^m h\Delta t z^{-1}}{2(1-z^{-1})}\right)\cdot(U_0 + U_1 z^{-1} + U_2 z^{-2} + \cdots) \tag{47}$$

$$W_0^m(z)\cdot(1-z^{-1}) = (W_{0,0}^m + W_{0,1}^m z^{-1} + W_{0,2}^m z^{-2} + \cdots)(1-z^{-1}) = \\ = \left(A_0^m\Delta t z^{-1} + \frac{A_0^m h\Delta t z^{-1}}{2}\right)\cdot(U_0 + U_1 z^{-1} + U_2 z^{-2} + \cdots) \tag{48}$$

The polynomials, at both member sides, must be equal. Thus their coefficients must also be equal. Only the coefficient of z^{-1} is required for the SST method:

$$(W_{0,1}^m - W_{0,0}^m) = \left(A_0^m\Delta t U_0 + \frac{A_0^m\Delta t}{2} h U_0\right) \tag{49}$$

but since $hU_0 = U_1 - U_0$:

$$W_{0,1}^m = W_{0,0}^m + A_0^m \Delta t \frac{(U_0 + U_1)}{2} \tag{50}$$

Analogously, for the other states W_k^m:

$$\begin{aligned} &W_k^m(z) = W_{k,0}^m + W_{k,1}^m z^{-1} + W_{k,2}^m z^{-2} + \cdots = \\ &= \left[A_k^m \frac{\left[\alpha_k \Delta t(1 - e^{-\alpha_k \Delta t}) + h(\alpha_k \Delta t - 1 + e^{-\alpha_k \Delta t})\right] z^{-1}}{\alpha_k^2 \Delta t(1 - e^{-\alpha_k \Delta t} z^{-1})} \right] \cdot \\ &\cdot (U_0 + U_1 z^{-1} + U_2 z^{-2} + \cdots) \end{aligned} \tag{51}$$

$$\begin{aligned} &W_k^m(z) \cdot (1 - e^{-\alpha_k \Delta t} z^{-1}) = (W_{k,0}^m + W_{k,1}^m z^{-1} + W_{k,2}^m z^{-2} + \cdots)(1 - e^{-\alpha_k \Delta t} z^{-1}) = \\ &= \left[A_k^m \frac{\left[\alpha_k \Delta t(1 - e^{-\alpha_k \Delta t}) + h(\alpha_k \Delta t - 1 + e^{-\alpha_k \Delta t})\right] z^{-1}}{\alpha_k^2 \Delta t} \right] \cdot \\ &\quad \cdot (U_0 + U_1 z^{-1} + U_2 z^{-2} + \cdots) \end{aligned} \tag{52}$$

by focusing on the coefficient of z^{-1}, i.e., how the state evolves, and by using $hU_0 = U_1 - U_0$:

$$W_{k,1}^m = W_{k,0}^m \cdot e^{-\alpha_k \Delta t} + \frac{A_k^m}{\alpha_k^2 \Delta t} \left[(1 - (1 + \alpha_k \Delta t) e^{-\alpha_k \Delta t}) U_0 + (\alpha_k - 1 + e^{-\alpha_k \Delta t}) U_1\right] \tag{53}$$

Eqs. (50) and (53) just tell us how any state, in this case, evolves over time from one sampling point to the next.

Nevertheless, to calculate how the superficial temperature changes, i.e., ΔT, from a sampling time point (labeled 0) to the next (labeled 1), the difference in the output-signals $V_1 - V_0$ is used instead. Therefore, the difference between the coefficients of z^{-1} and z^0 is computed as:

$$V_1 = W_{0,1}^m + \sum_{k=1}^{\infty} W_{k,1}^m \tag{54}$$

$$V_0 = W_{0,0}^m + \sum_{k=1}^{\infty} W_{k,0}^m \tag{55}$$

that is:

$$\begin{aligned} &\Delta V = V_1 - V_0 = W_{0,1}^m - W_{0,0}^m + \sum_{k=1}^{\infty} (W_{k,1}^m - W_{k,0}^m) \\ &\Delta V = V_1 - V_0 = A_0^m \Delta t \frac{(U_0 + U_1)}{2} + \sum_{k=1}^{\infty} (W_{k,1}^m - W_{k,0}^m) \end{aligned} \tag{56}$$

where the terms between brackets, taking into account (53) have the form:

$$\begin{aligned} &W_{k,1}^m - W_{k,0}^m = \\ &- W_{k,0}^m (1 - e^{-\alpha_k \Delta t}) + \frac{A_k^m}{\alpha_k^2 \Delta t} \left[(1 - (1 + \alpha_k \Delta t) e^{-\alpha_k \Delta t}) U_0 + (\alpha_k - 1 + e^{-\alpha_k \Delta t}) U_1\right] \end{aligned} \tag{57}$$

At this point, the following points should be stressed:

- Eqs. (56) and (57) allow us to compute $\Delta V = \Delta T^m$ for a certain output–input couple labeled by m. The linear composition means that the actual changes on either side are given by:

$$\Delta T_0 = \Delta T^{00} + \Delta T^{01} \tag{58}$$

$$\Delta T_1 = \Delta T^{10} + \Delta T^{11} \tag{59}$$

- *However the states evolve as Eqs.* (50) and (53) *show.*

The final expressions, similar to the ones in the previous section, are the following. Labeling the change of T at the 0-side, as ΔT_0. Eq. (58) leads to:

$$\begin{aligned} \Delta T_{0,(n)} = &A_0^{00} \Delta t \frac{(\dot{q}_{0,(n-1)} + \dot{q}_{0,(n)})}{2} + \sum_{k=1}^{\infty} (W_{k,(n)}^{00} - W_{k,(n-1)}^{00}) + \\ &+ A_0^{01} \Delta t \frac{(\dot{q}_{1,(n-1)} + \dot{q}_{1,(n)})}{2} + \sum_{k=1}^{\infty} (W_{k,(n)}^{01} - W_{k,(n-1)}^{01}) \end{aligned} \tag{60}$$

where now (n) and $(n-1)$ are the current and previous sampling points, respectively. Using (57):

$$\begin{aligned}\Delta T_{0,(n)} =& \frac{(A_0^{00}\dot{q}_{0,(n-1)} + A_0^{01}\dot{q}_{1,(n-1)})}{2}\Delta t + \frac{(A_0^{00}\dot{q}_{0,(n)} + A_0^{01}\dot{q}_{1,(n)})}{2}\Delta t + \\ &+ \sum_{k=1}^{\infty} -\overbrace{(W_{k,(n-1)}^{00} + W_{k,(n-1)}^{01})}^{W_{k,(n-1)}^{0}}(1-e^{-\alpha_k\Delta t}) + \\ &+ \sum_{k=1}^{\infty}\left[\frac{A_k^{00}}{\alpha_k^2\Delta t}(1-(1+\alpha_k\Delta t)e^{-\alpha_k\Delta t})\dot{q}_{0,(n-1)} + \frac{A_k^{01}}{\alpha_k^2\Delta t}(1-(1+\alpha_k\Delta t)e^{-\alpha_k\Delta t})\dot{q}_{1,(n-1)}\right] + \\ &+ \sum_{k=1}^{\infty}\left[\frac{A_k^{00}}{\alpha_k^2\Delta t}(\alpha_k - 1 + e^{-\alpha_k\Delta t})\dot{q}_{0,(n)} + \frac{A_k^{01}}{\alpha_k^2\Delta t}(\alpha_k - 1 + e^{-\alpha_k\Delta t})\dot{q}_{1,(n)}\right]\end{aligned} \tag{61}$$

where W_k^0 is the "full" state at the 0-side. Due to the linearity of the physical model, it is just the sum of the "partial" states. Analogously to the previous case, three secondary parameters are defined (notice that there is one more than before):

$$\varphi_k = e^{-\alpha_k\Delta t} \tag{62a}$$

$$r_{T,k} = \frac{1-(1+\alpha_k\Delta t)e^{-\alpha_k\Delta t}}{\alpha_k^2\Delta t} \tag{62b}$$

$$p_{T,k} = \frac{\alpha_k - 1 + e^{-\alpha_k\Delta t}}{\alpha_k^2\Delta t} \tag{62c}$$

and by using Eq. (61), the next two linear equations are obtained:

$$\Delta T_{0,(n)} = a_T^{00}\cdot\dot{q}_{0,(n)} + a_T^{01}\cdot\dot{q}_{1,(n)} + d_T^0 \tag{63a}$$

$$\Delta T_{1,(n)} = a_T^{10}\cdot\dot{q}_{0,(n)} + a_T^{11}\cdot\dot{q}_{1,(n)} + d_T^1 \tag{63b}$$

where:

$$a_T^m = \frac{A_0^m}{2} + \sum_{k=0}^{\infty} p_{T,k}\cdot A_k^m \tag{64a}$$

$$\begin{aligned} d_T^0 =& \sum_{k=1}^{\infty} -W_{k,(n-1)}^0\cdot(1-\varphi_k) + \\ &+ \left(\frac{A_0^{00}}{2} + \sum_{k=1}^{\infty} r_{T,k}\cdot A_k^{00}\right)\cdot\dot{q}_{0,(n-1)} + \left(\frac{A_0^{01}}{2} + \sum_{k=1}^{\infty} r_{T,k}\cdot A_k^{01}\right)\cdot\dot{q}_{1,(n-1)} \\ d_T^1 =& \sum_{k=1}^{\infty} -W_{k,(n-1)}^1\cdot(1-\varphi_k) + \\ &+ \left(\frac{A_0^{10}}{2} + \sum_{k=1}^{\infty} r_{T,k}\cdot A_k^{10}\right)\cdot\dot{q}_{0,(n-1)} + \left(\frac{A_0^{11}}{2} + \sum_{k=1}^{\infty} r_{T,k}\cdot A_k^{11}\right)\cdot\dot{q}_{1,(n-1)} \end{aligned} \tag{64b}$$

The successive k-state transitions at both sides W_k^0 and W_k^1, are given by:

$$\begin{aligned} W_{k,(n)}^0 &= W_{k,(n)}^{00} + W_{k,(n)}^{01} \\ W_{k,(n)}^0 &= W_{k,(n-1)}^0\cdot\varphi_k + \\ &+ p_{T,k}\cdot(A_k^{00}\cdot\dot{q}_{0,(n)} + A_k^{01}\cdot\dot{q}_{1,(n)}) + r_{T,k}\cdot(A_k^{00}\cdot\dot{q}_{0,(n-1)} + A_k^{01}\cdot\dot{q}_{1,(n-1)}) \end{aligned} \tag{65a}$$

$$\begin{aligned} W_{k,(n)}^1 &= W_{k,(n)}^{10} + W_{k,(n)}^{11} \\ W_{k,(n)}^1 &= W_{k,(n-1)}^1\cdot\varphi_k + \\ &+ p_{T,k}\cdot(A_k^{10}\cdot\dot{q}_{0,(n)} + A_k^{11}\cdot\dot{q}_{1,(n)}) + r_{T,k}\cdot(A_k^{10}\cdot\dot{q}_{0,(n-1)} + A_k^{11}\cdot\dot{q}_{1,(n-1)}) \end{aligned} \tag{65b}$$

4. Discussion

Though the paper aims to present the fundamentals of this new methodology, not the details of its efficient implementation, some discussion is advisable. In our opinion, some additional research could significantly improve its performance.

The previous sections show the new formulation that always takes the conduction heat flux $\dot{q}$ as the input signal, while conventionally, this was the output one. Chiefly, our response target is the rate of change $\dot{T}$ of the superficial temperatures. Nevertheless, Section 3.3 tackles the case of finding out ΔT, as well. In any case, the outcome is just a pair of linear equations; Eqs. (36) and (63), respectively. Roughly, the difficulty relies on how to compute the coefficients of that system.

The procedure follows the next steps:

Table 1
Physical properties of the example-wall layers. Overall: $U = 0.45$ [W/m^{2}K], $L_{total} = 0.23$ [m], $C_{total} = 385.6$ [kJ/m^{2}K], specific weight 307 [kg/m^2].

Pos.	k [W/mK]	ρ [kg/m^3]	c_p [J/kgK]	L [m]	R [m^{2}K/W]	C [kJ/m^{2}K]
1	0.870	1800	1380	0.120	0.1379	2980.8
2	1.400	2000	1050	0.015	0.0107	31.5
3	0.033	25	837	0.040	1.2121	0.8
4	0.049	1200	920	0.040	0.8183	44.2
5	0.300	800	920	0.015	0.0500	11.0

1. Given a slab composition, a number K of poles α_k and residues A_k^m must be calculated ($k < K$). Recall that the impulsion time-response (see Eq. (11)) shows that the slab has an infinite number of response modes (states) that decay exponentially. The quicker the decay, the bigger α_k of the mode. This number K depends on the shortest time Δt_{min} for which the method should be able to compute a response and, of course, on the properties of the slab.
   In practice, the original Japanese SST method [14], used a maximum amount $k_{max} < K$ of poles. The terms associated with the difference $K - k_{max}$ were employed to reduce the impulse time response (like, for instance, Eq. (11)) to a finite series plus a correction term. However, this term is not included here for exposition clarity, since it does not affect the essentials. It is assumed that enough poles are used to build an accurate response.
2. Initialization: at $n = 0$, all temperatures, their states and the inputs $\dot{q}_{0,0\equiv n}$ and $\dot{q}_{1,0\equiv n}$ are zero.
3. Next, current step becomes the previous one $(n-1) \leftarrow n$. After a Δt, new heat fluxes $\dot{q}_{0,n}$, $\dot{q}_{1,n}$ have been sampled.
   (a) Calculate the coefficients $\{a^m\}$ or $\{a_T^m\}$, $m \in \{00, 01, 10, 11\}$ and the independent terms $\{d^0, d^1\}$ or $\{d_T^0, d_T^1\}$ by using Eqs. (38) or (64), in order to compute the response $\dot{T}$ or ΔT, respectively.
   (b) Notice that the independent terms depend on the previous superficial states: $w_{k,(n-1)}^m$, or $W_{k,(n-1)}^m$, for $\dot{T}$ or ΔT, respectively.
   (c) There are several other secondary parameters indexed by k; $\{\varphi_k\}$ common to $\dot{T}$ or ΔT response, and one specific $\{r_k\}$ for the $\dot{T}$, and two $\{r_{T.k}, p_{T,k}\}$ for ΔT.
   The example section and Appendix B.2 illustrate that these parameters go to zero as α_k and Δt increase. It is obvious for $\varphi_k = e^{-\alpha_k \Delta t}$. In other words, if the elapsed time between transitions is short, many states are excited, which must be retained between evolution calls to build the response. In an event-driven simulation, this situation would correspond to a high superficial $\dot{T}$. On the contrary, if Δt is long (i.e., T changes slowly), many states go to zero (i.e., disappear) and have a negligible effect on the response. Otherwise stated, with fewer states, it is possible to estimate the response after Δt.
   One possible criterion, already successfully used in [15], was the following. Before computing everything, that is; the coefficients, the independent terms, and the successive state transition, the following quick check is made: $\varphi_k < Tol$. For instance, take $Tol = 10^{-10}$. Thus it may be assumed that,

$$\forall \quad k > k_{transition-max} \rightsquigarrow \varphi_k \approx 0 \tag{66}$$

   along with all the other corresponding secondary k-parameters. Clearing from $\varphi_k < Tol$, the threshold $k_{transition-max}$ would be found from:

$$\alpha_{k_{transition-state}} > \frac{10\ln(10)}{\Delta t} \tag{67}$$

4. Compute the SST evolution: update only those states $k \le k_{transition-max}$, while those corresponding to $k > k_{transition-max}$ are set to zero directly or simply deleted.
5. If a new event requires the computation of $\dot{T}$ or ΔT due to a new conduction heat flux input-event, then go to step 3.

Next section illustrates all the previous outcomes with a concrete example.

5. Calculation: example wall

Table 1 describes the properties of a multi-layered wall, also illustrated in Fig. 7.

This wall has a thermal conductivity $U = 0.45\,[\mathrm{W/m^2K}]$, total thickness $L_{total} = 0.23\,[\mathrm{m}]$, and a heat capacity per m^2 $C_{total} = 385,6\,[\mathrm{kJ/m^2K}]$. Its weight is $307\,[\mathrm{kg/m^2}]$. Thus, it is a medium or heavy wall attending to its properties. Recall that the bigger the pole (in absolute value, i.e., α_k), the quicker the wall's response mode.

The example wall has 4729 poles such that $\alpha_k < 500$. However, Appendix B shows only the first 50 and their corresponding residues. For practical uses, 50 is more than enough. Nevertheless, more than 50 was used to create the following Figures, illustrating the new ideas. Incidentally, the poles/residues computation relies on a fast algorithm based on [16,17].

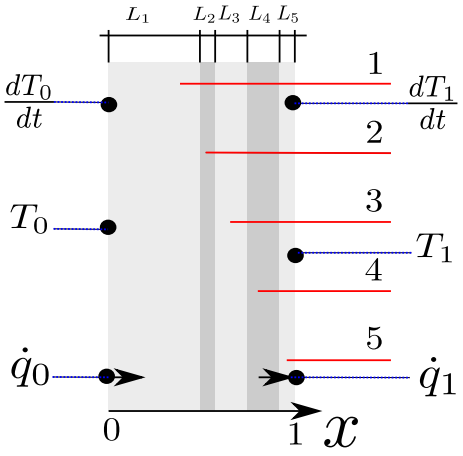

Fig. 7. Scheme of the example wall layers. Remark: 0 means outside, 1 inside.

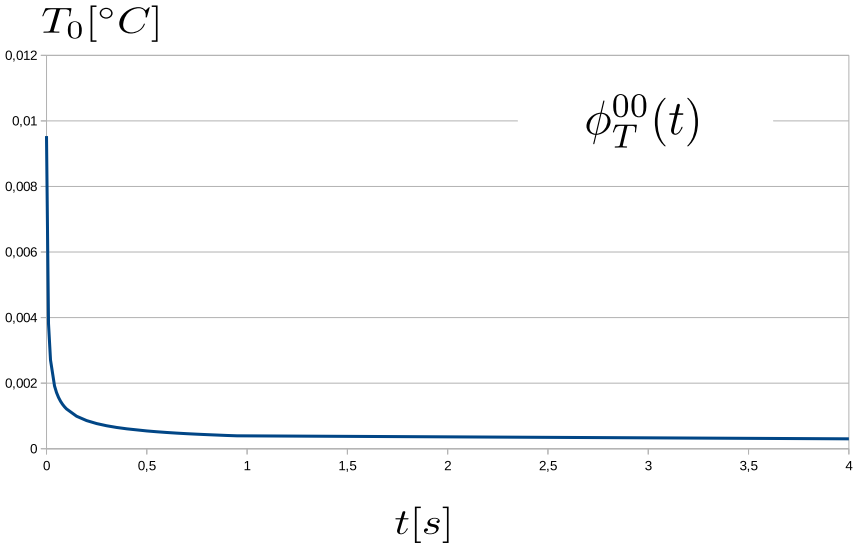

Fig. 8. `Impulse` response of $T_0(t)$ to a conduction heat flux $\dot{q}_0 = \delta(t)$, at 0-side, of the example wall.

5.1. *T response to an impulse $\dot{q}$*

First, to understand our new CFT, the temperature time response to an impulse conduction heat flux $\dot{q}$ is sought. If the excitation is on the 0-side, then Fig. 8 shows the response on the same side. Logically, in $t = 0$ the summation $\sum_{k=1}^{\infty} A_k^{00}$ of Eq. (11) does not converge. After receiving heat ($\dot{q}_0 = \delta(t)\,[\mathrm{W/m^2}]$), the superficial temperature at the same side goes to infinity, as expected. The response is very rapid during the first $t = 1\,[\mathrm{s}]$. Nevertheless, due to the scale in Fig. 8, the steady state seems to be reached very soon, but it takes several hours. If $t \to \infty$ Eq. (11) tends to A_0^{00}, i.e., to a constant temperature value that depends on the wall properties. Looking at Appendix B, its value is 0.00000259324666703 (the residue at $\alpha_0 = 0$). This temperature value will be the same at any point within the wall at the end of the process. Notice that the excitation is an *injection* of heat, concretely in Fig. 8: at 1-side $\dot{q}_1(t) = 0$ for $t \geq 0$, i.e., that side is always adiabatic, while 0-side receives a "sudden" heat impulse $\delta(t)$ (Kronecker's delta), and thereafter it is always $\dot{q}_0(t) = 0$ for $t > 0$, that is, it becomes adiabatic once more.

Fig. 9, shows the T response at the opposite side 1 to the same heat impulse $\dot{q}_0 = \delta(t)$, as before. Initially, there is no response, but after a while (around 1 [h]), T_1 starts rising until it reaches a stationary value. Notice that $A_0^{10} = A_0^{00}$ (see Appendix B). It takes long, roughly 24 [h], to reach 80% of its final value, due to the high weight of the wall. An interesting feature is that, according to

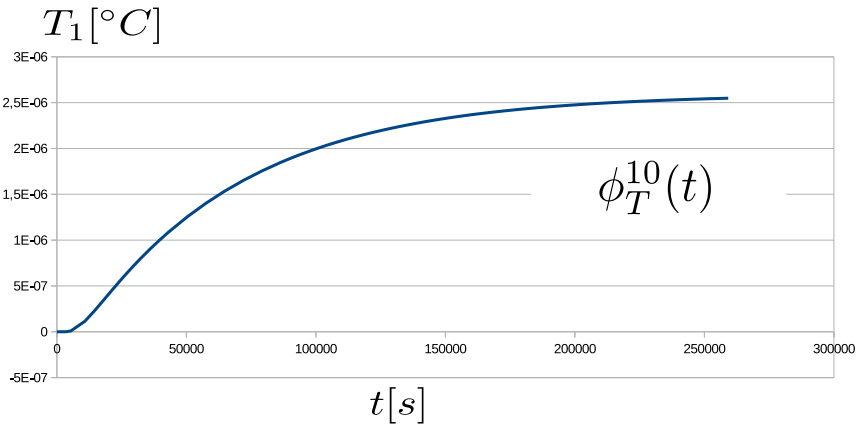

Fig. 9. Impulse $T_1(t)$ response to $\dot{q}_0 = \delta(t)$ for the example wall.

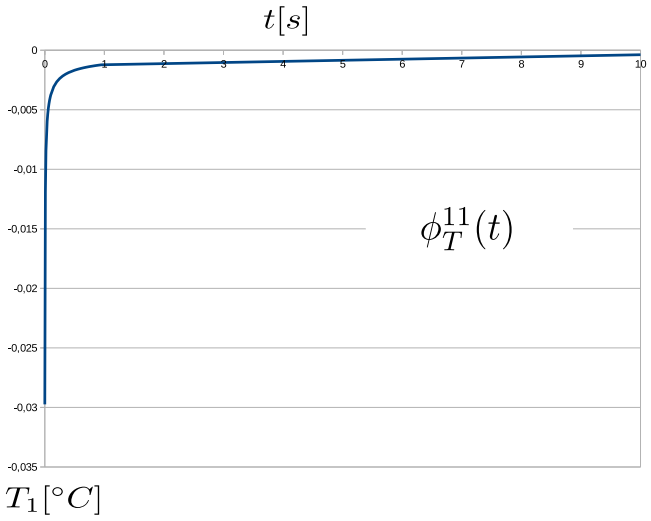

Fig. 10. Impulse $T_1(t)$ response to $\dot{q}_1 = \delta(t)$, for the example wall.

Fig. 9, at $t = 0$, Eq. (11) must sum zero. Therefore, the next must be true:

$$A^{10} + \sum_{k=1}^{\infty} A_k^{10} = 0 \tag{68}$$

The response $\phi_T^{01}(t)$ (not represented), is similar to $\phi_T^{10}(t)$, but with opposite sign. It is so because the heat impulse $\dot{q}_1 = \delta(t)$ is now a *heat extraction* (see the positive x-axis). Thus, it creates a temperature decrease in the whole wall.

Finally, Fig. 10 shows the response $\phi_T^{11}(t)$. Logically, since $\dot{q}_1 = \delta(t)$ removes energy from the wall, the temperature has a similar behavior than $\phi_T^{00}(t)$. However, the response on this side is quicker than $\phi_T^{00}(t)$. The cause is that this side has a smaller heat capacity.

Next section illustrates also this asymmetric behavior for this particular example case.

5.2. Successive state transition: example

The previous section showed the wall state evolution to what perturbs its thermodynamic equilibrium; the conduction heat fluxes $\dot{q}$ *imposed* at both sides. Now, the developed SST method is applied to illustrate the superficial responses: $\dot{T}$ and T.

Appendix B.2 shows for $\Delta t = 10\,[\text{min}]$ and $\Delta t = 60\,[\text{min}]$, the number of poles used, according to the criterion of Section 4. In concrete, that number varies with $\alpha_k \Delta t$.

As instances, two wall excitation cases are posed. In both, $\dot{q}_0(t) = \dot{q}_1(t)$ just to make the exposition simple.

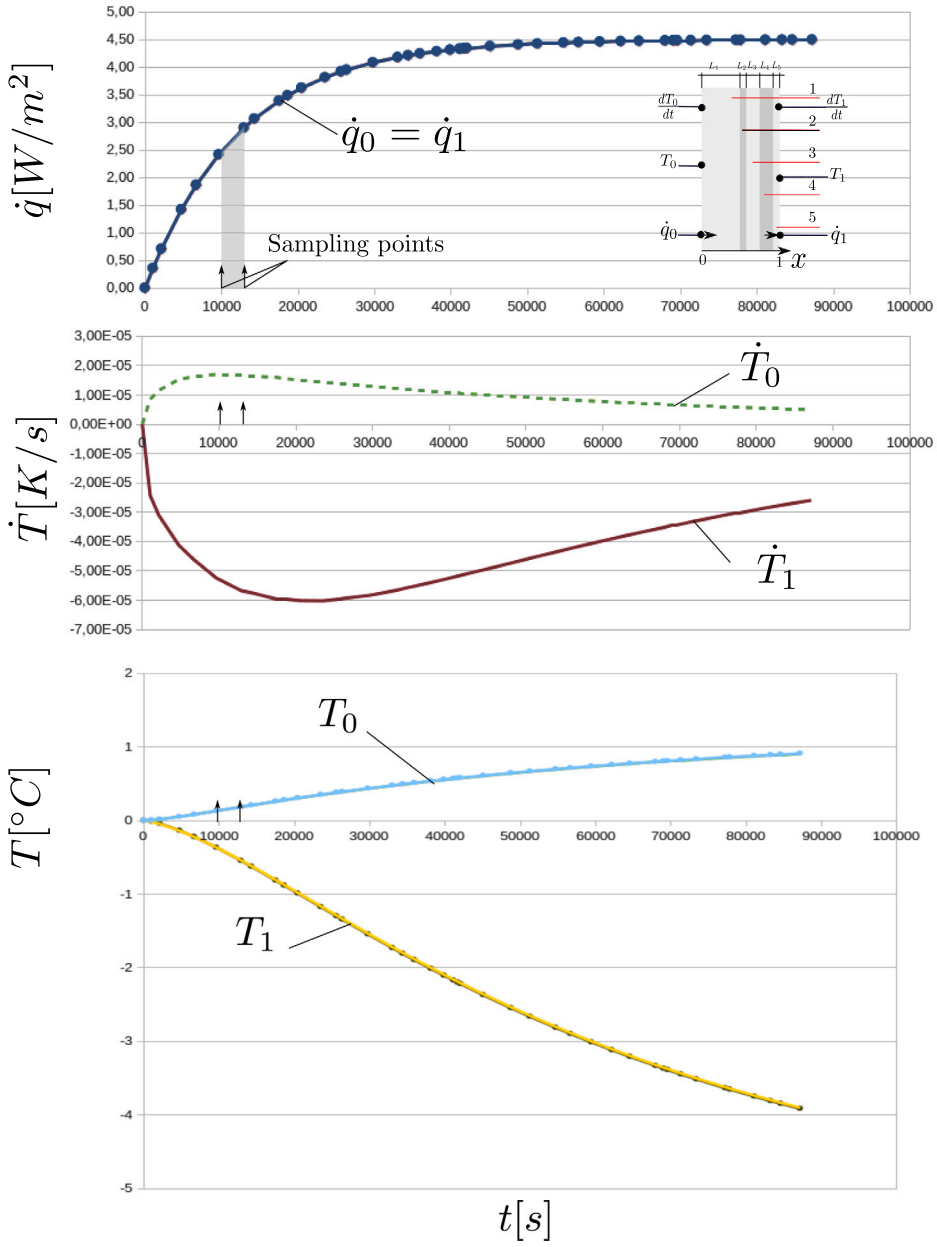

Fig. 11. Example wall response to case 1 (see Appendix B.3). Top: heat fluxes sampled at the solid circles, i.e., sampling points where $\dot{T}$ and T values are also computed. However, on the other two graphs, lines connect them to grasp the expected profiles.

- *Case* 1: the aim here is to mimic a sort of sudden transition process. It increases the heat fluxes at the same rate, from zero up to a constant value of $\dot{q} = 4.5\,[\mathrm{W/m^2}]$. At approximately 14 [h], they reach 90% of this latter value, and the calculation proceeds until 24 [h]. The sampling time points have been chosen randomly with an arbitrarily selected minimum elapsed time of 5 [min].
  Appendix B.3 shows the employed values. As discussed, the holder element forces a linear heat flux profile between sampling points.
  Fig. 11 displays the result. On top, the heat flux appears with a solid circle marking the sampling points.
  The graph in the middle displays the superficial temperature velocities $\dot{T}$. Initially, both T speeds are null, rise to a maximum, and then go back to zero since the wall is reaching its steady state of heat conduction. Notice that $\dot{T}_0 > 0$ but $\dot{T}_1 < 0$: that is,

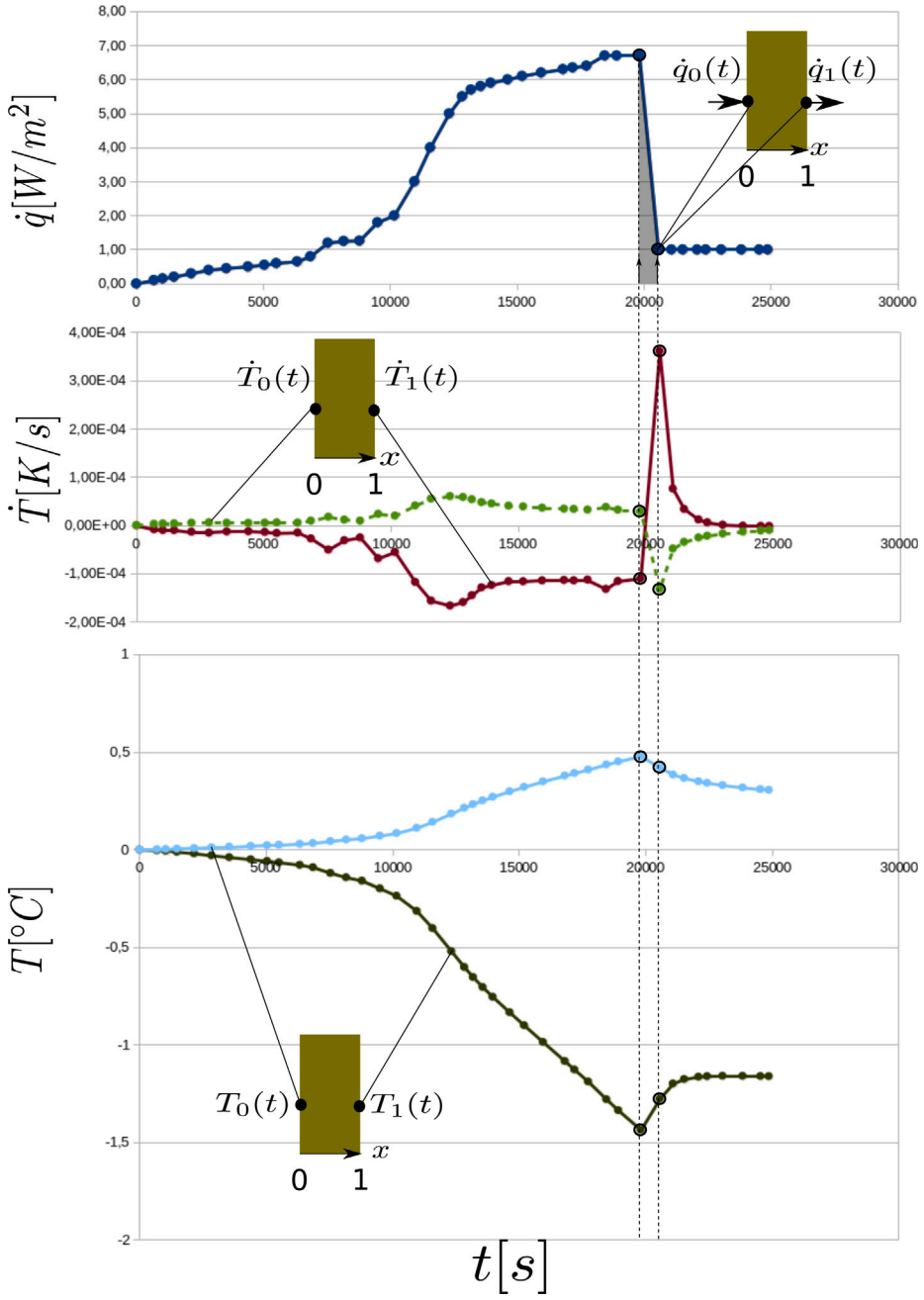

Fig. 12. Example wall response to case 2. $\dot{T}$ and T are only known at sampling points.

0-side is warming up (is receiving heat), while 1-side is cooling down (heat is removed). The speed at 0-side is lower than at 1-side due to the unsymmetrical physical properties (see Table 1) of the wall at either side.

Finally, the bottom graph shows the T on both sides. Initially, the whole wall was set to $T = 0$ [°C], but it could be any other value since the model evaluates how it changes its state over time, i.e., the ΔT evolution between samples. Since the overall thermal conductivity of the wall is $U = 0.45$ [W/m^{2}K] (see Table 1), the steady-state temperature difference between both sides will be 10 [°C]. Looking at the Figure, after 24 [h] of the randomly chosen heating process, the temperature difference is around 5 [°C]. Based on its thermal inertia (related to the RC value), this heavy wall would take around 35 [h] to approach its steady state.

- *Case* 2: the aim now is to mimic a case where, after some random and rising excitation path of the $\dot{q}$, the wall suffers a sudden deviation, in the opposite direction. As before, both heat fluxes moved symmetrically up and down and were randomly chosen. Table B.4 shows the heat flux values. The sampling time-points have also been selected randomly with no intention of emulating an event-driven simulation. A minimum of 5 [min] separates the sampling points.
  The upper graph in Fig. 12 displays how the heat fluxes evolve. The heat fluxes are abruptly reduced after a while, or in other words, the wall suddenly "becomes more adiabatic", so to say.
  The middle graph shows the $\dot{T}$ at the sampled points. Notice that the high flux acceleration also changes significantly the temperature speeds. Even they exchange their signs: the 0-side decreases its temperature as heat flows to the right while the 1-side one rises since it receives heat from the left while that side boundary condition becomes closer to "adiabatic" (reduced $\dot{q}$).
  Finally, the bottom graph shows, as before, the T on both sides. It is noteworthy that the T responses are the "exact" outcomes, not approximations, to the applied heat fluxes. Therefore, regardless of Δt, the possible exponential-like T responses are retained by the procedure. This T behavior differs entirely from the traditional approach.

6. Conclusions

The building energy simulation realm has been evolving quickly in the last decade due to the new requirements imposed by the energy and climate crisis on engineering. The trend is to move onto a discrete event simulation rather than to remain within the time perspective. Recent studies show that even fundamental aspects might need to be dealt with correctly in our current methods and procedures. This problem is also known as *the building energy performance gap*. The paper tries to make a small step forward.

Concretely, it tackles the multi-layered slab $1D$ conduction heat transfer calculation. Historically, there are two approaches: the finite difference and the conduction transfer function method, or CTF, for short. They had remained basically untouched for more than 50 years. Undoubtedly, they are very useful. Nevertheless, they do not fit the current simulation trends and need an upgrade or a rethink. Based on previous results [13], this paper considers a new transfer function: one that relates the conduction heat flux $\dot{q}$ at both sides of the element to the speed of its superficial temperatures $\dot{T}$. In contrast, the traditional method takes T as inputs and $\dot{q}$ as outputs. But, additionally, the solution procedure should fit better in a discrete event simulation paradigm. So, instead of using Mitalas' method, the paper recovers a somewhat forgotten one from the Japanese literature: the *successive state transition method*, or briefly *SST*. The linear Eq. (38) and the successive state transition rules given by Eqs. (39) and (40), summarize the solution. Additionally, Eq. (37) provide a suitable secondary set of parameters that aid us in establishing the solution procedure.

Moreover, the paper shows that the same SST methodology can be used to obtain the *exact T responses* to heat input $\dot{q}$ pulses on both sides. It is indirectly possible through the temperature difference ΔT. Now, the linear Eq. (63) along with Eq. (64) and the successive state transition rules (65) define the solution. Analogously to the previous case, Eq. (62) gather the suitable auxiliary parameters which help establishing the solution procedure.

The method has the following features:

- *Variable time steps* with conduction transfer functions.
- Knowing $\dot{T}$ allows us to track the wall state, thus allowing scheduling more frequent events for those fast-evolving walls. In simple terms: *it fits an event-driven simulation* of the building's solid parts. Thus a fully event-driven building simulation is enabled.
- Additionally, the paper shows how to compute the T response. Therefore, *it allows us to estimate the process variables* (heat exchange fluxes) more accurately.
  Moreover, this has implications for improving QSS methods (Quantized State System) used in discrete event simulation of continuous systems (see [18]).
- Since, contrary to the conventional method, the energy input into the wall is known, the simulations could be more physically consistent. In other words, *it contributes to reducing the energy performance gap*.
- Recall that the evolution of the superficial temperatures is not forced or imposed, as in the traditional method. Thus, it allows a *better indoor comfort estimation*.
  Incidentally, this is an increasing importance target due to the climate change and energy crisis resilience challenges.
- *The computational burden is adaptive.* When the time sampling points are closer (i.e., small Δt)), the effort rises, and vice versa. This trade-off does not occur with the finite difference models or with the fixed time-step methods. Our procedure uses, in practice, a *variable* quantity of internal states to build the response. This amount depends roughly on each Δt and on the physical properties of the element.
- *The proposed method can use as much information as needed* about the thermal response of the element. Beforehand, the user must define the smallest Δt for which the method should deliver a response. Then all the required information is computed and used adaptively according to the actual elapsed time between heat flux events.

This new method of dealing with the 1D conduction heat transfer in multi-layered walls adds the complexity of computing the poles and residues inherent to any root-finding method. Besides, the SST method has a particularity; it needs the evaluation of costly exponential functions.

Future research will use the proposed methodology and the discrete event specification scheme to analyze its practical application in building energy simulation (i.e., similar to our previous work [13]).

CRediT authorship contribution statement

Víctor Manuel Soto Francés: Conceptualization, Formal analysis, Methodology, Software, Writing. **José Manuel Pinazo Ojer:** Conceptualization, Validation, Review. **Emilio José Sarabia Escrivá:** Software, Visualization, Review.

Declaration of competing interest

The authors declare the following financial interests/personal relationships which may be considered as potential competing interests: Victor Manuel Soto Frances reports article publishing charges was provided by CRUE-Universitat Politécnica de Valéncia.

Data availability

No data was used for the research described in the article.

Acknowledgments

This study has not received any dedicated financial support. Funding for open access charge: CRUE-Universitat Politècnica de València.

Appendix A. Traditional CTF

Starting with the well-known expressions for the conventional $\mathcal{G}^m(s)$ in Eq. (2). For a single layer characterized by its thickness L, thermal diffusivity α and thermal conductivity k:

$$\mathcal{G}^{00}(s) = k\sqrt{s/\alpha}\cdot\frac{\cosh(L\sqrt{s/\alpha})}{\sinh(L\sqrt{s/\alpha})} \tag{A.1a}$$

$$\mathcal{G}^{01}(s) = -k\sqrt{s/\alpha}\cdot\frac{1}{\sinh(L\sqrt{s/\alpha})} = -\mathcal{G}^{10}(s) \tag{A.1b}$$

$$\mathcal{G}^{11}(s) = -k\sqrt{s/\alpha}\cdot\frac{\cosh(L\sqrt{s/\alpha})}{\sinh(L\sqrt{s/\alpha})} \tag{A.1c}$$

Usually, the literature uses the following terminology:

$$R = L/k \tag{A.2a}$$

$$M(s) = L\sqrt{s/\alpha} = \sqrt{L^2\cdot 1/(k/(\rho c_p))}\cdot\sqrt{s} = \sqrt{RC}\cdot\sqrt{s} \tag{A.2b}$$

$$C = \rho\cdot c_p\cdot L \tag{A.2c}$$

where R is the thermal resistance, M is the thermal inertia and C the thermal capacity per m^2. To compose the multi-layered slab, Eq. (2) is not useful. The conditions on one side $\{T,\ \dot{q}\}$ must be related to the ones on the other:

$$\begin{bmatrix}\mathcal{L}T_1\\ \mathcal{L}\dot{q}_1\end{bmatrix} = \begin{bmatrix}A(s) & -B(s)\\ -C(s) & D(s)\end{bmatrix}\cdot\begin{bmatrix}\mathcal{L}T_0\\ \mathcal{L}\dot{q}_0\end{bmatrix}, \tag{A.3}$$

where using Eq. (A.2):

$$A(s) = \cosh M(s) = D(s) \tag{A.4a}$$

$$B(s) = R\cdot\sinh M(s)/M(s) \tag{A.4b}$$

$$C(s) = \frac{1}{R}\cdot M(s)\sinh M(s) \tag{A.4c}$$

Eq. (A.3) can also be transformed into (swapping 0 for 1):

$$\begin{bmatrix}\mathcal{L}T_0\\ \mathcal{L}\dot{q}_0\end{bmatrix} = \begin{bmatrix}A(s) & B(s)\\ C(s) & D(s)\end{bmatrix}\cdot\begin{bmatrix}\mathcal{L}T_1\\ \mathcal{L}\dot{q}_1\end{bmatrix} \tag{A.5}$$

If the layer sequence is taken as in Fig. 1, i.e., from outside 0 (layer 1) to inside 1 (layer n), the multi-layered matrix is obtained by multiplication as:

$$\begin{bmatrix}\mathcal{L}T_0\\ \mathcal{L}\dot{q}_0\end{bmatrix} = \begin{bmatrix}A(s) & B(s)\\ C(s) & D(s)\end{bmatrix}_n\cdot\begin{bmatrix}A(s) & B(s)\\ C(s) & D(s)\end{bmatrix}_{n-1}\cdots\begin{bmatrix}A(s) & B(s)\\ C(s) & D(s)\end{bmatrix}_1\cdot\begin{bmatrix}\mathcal{L}T_1\\ \mathcal{L}\dot{q}_1\end{bmatrix} \tag{A.6}$$

$$\begin{bmatrix}\mathcal{L}T_0\\ \mathcal{L}\dot{q}_0\end{bmatrix} = \begin{bmatrix}AA(s) & BB(s)\\ CC(s) & DD(s)\end{bmatrix}\cdot\begin{bmatrix}\mathcal{L}T_1\\ \mathcal{L}\dot{q}_1\end{bmatrix} \tag{A.7}$$

and clearing for the heat fluxes:

$$\begin{bmatrix} \mathcal{L}\dot{q}_0 \\ \mathcal{L}\dot{q}_1 \end{bmatrix} = \begin{bmatrix} DD(s)/BB(s) & -1/BB(s) \\ 1/BB(s) & -AA(s)/BB(s) \end{bmatrix} \cdot \begin{bmatrix} \mathcal{L}T_0 \\ \mathcal{L}T_1 \end{bmatrix} \tag{A.8}$$

Eq. (A.8) is a more explicit form of (Eq. (2)).

Appendix B. Example wall

B.1. Poles and residues at the poles

For the example wall, this section contains its computed poles and residues.
Residues for $k = 0$ ($\alpha_0 = 0$):

$$A_0^{00} = 0.00000259324666703 \tag{B.1}$$

$$A_0^{10} = 0.00000259324666703 \tag{B.2}$$

$$A_0^{11} = -0.00000259324666703 \tag{B.3}$$

the next Table B.2 are the first 50 poles α_k and their residues $k \geq 1$:

Table B.2
Values ordered top-down from $k = 1 \ldots 50$.

α_k	A_k^{00}	A_k^{10}	A_k^{11}
1.62E−05	5.78E−07	−3.03E−06	−1.59E−05
5.33E−05	−6.43E−19	7.30E−18	8.29E−17
2.01E−04	5.98E−06	5.95E−07	−5.92E−08
2.98E−04	3.03E−16	2.94E−17	−2.85E−18
4.48E−04	2.31E−18	−3.36E−17	−4.88E−16
7.93E−04	6.09E−06	−3.56E−07	−2.08E−08
1.24E−03	3.08E−18	2.20E−16	−1.57E−14
1.63E−03	5.47E−08	1.68E−06	−5.15E−05
1.79E−03	6.09E−06	−1.63E−06	−4.34E−07
2.44E−03	−1.38E−17	5.50E−16	2.19E−14
3.04E−03	−3.83E−14	−1.98E−15	1.03E−16
3.19E−03	6.18E−06	3.04E−07	−1.50E−08
4.05E−03	−2.98E−17	1.62E−15	8.78E−14
5.01E−03	6.17E−06	−1.35E−06	−2.94E−07
5.44E−03	3.59E−08	1.53E−06	−6.54E−05
6.08E−03	−3.30E−17	−1.98E−15	1.19E−13
7.24E−03	6.16E−06	−7.08E−07	−8.15E−08
8.45E−03	3.56E−15	−1.39E−14	−5.42E−14
8.85E−03	−2.02E−14	−1.35E−14	9.03E−15
9.46E−03	1.57E−06	2.49E−06	−3.95E−06
1.01E−02	4.81E−06	−2.73E−06	−1.55E−06
1.02E−02	1.24E−13	−5.59E−14	−2.52E−14
1.15E−02	−5.72E−16	−8.10E−15	1.14E−13
1.25E−02	1.89E−07	2.64E−06	−3.68E−05
1.30E−02	5.98E−06	−2.19E−06	−7.99E−07
1.47E−02	1.82E−17	−6.91E−16	−2.62E−14
1.64E−02	6.14E−06	2.59E−07	−1.09E−08
1.75E−02	−2.33E−13	−1.35E−14	7.80E−16
1.83E−02	2.07E−16	−3.55E−15	−6.07E−14
2.03E−02	6.10E−06	−3.14E−07	−1.62E−08
2.23E−02	−1.75E−16	−1.09E−14	6.77E−13
2.31E−02	1.60E−08	7.88E−07	−3.88E−05
2.45E−02	6.05E−06	−7.23E−07	−8.64E−08
2.67E−02	−7.58E−16	1.15E−14	1.74E−13
2.77E−02	3.10E−14	2.84E−15	−2.60E−16
2.90E−02	6.04E−06	3.54E−07	−2.07E−08
3.15E−02	8.00E−16	−3.00E−14	−1.13E−12
3.40E−02	5.90E−06	−1.84E−06	−5.74E−07
3.55E−02	1.51E−07	2.88E−06	−5.50E−05
3.65E−02	−6.31E−15	−9.70E−14	1.49E−12
3.86E−02	−1.61E−12	1.99E−12	2.45E−12
3.89E−02	2.88E−06	−4.60E−06	−7.37E−06
3.99E−02	3.40E−06	3.75E−06	−4.13E−06

B.2. Secondary parameters

This section illustrates how the value of the secondary parameters (37) and (62), for responses T and $\dot{T}$ respectively, vary with the absolute value of the pole α_k and the elapsed time Δt. In order to make the scales comparable, and since the value of all the secondary parameters go to zero with α_k, they are *normalized*, by dividing each value by its maximum absolute value (i.e., its value for α_1): for instance $\overline{\varphi_k} = \varphi_k/|\varphi_1|$, $\overline{r_{T,k}} = r_{T,k}/|r_{T,1}|$, and so on. Therefore, all the normalized values (denoted by an over-line) are in the interval $[-1, 1]$ (see Table B.2). Fig. B.13 shows the normalized values of the secondary parameters (62) (T response), for the example wall. The tolerance criterion of Section 4 is marked on its $\alpha_k \Delta t$ axis. It can be seen that, for short elapsed times, the amount of poles (states) which are taken into account is higher (40, for 10 min pulses in this example), while for longer ones only remain a few (16, for 1 h pulse in this example).

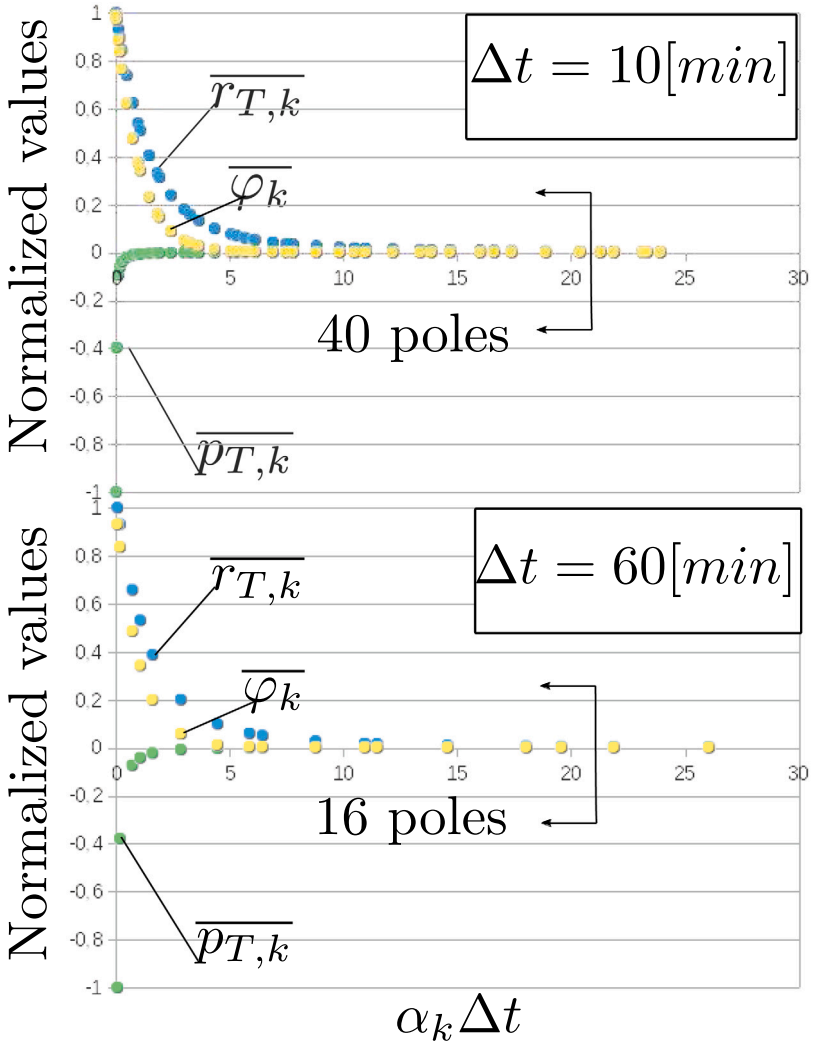

Fig. B.13. Secondary parameters for the T response, (62), applied to the example wall and for two different elapsed times Δt, short at the top and long at the bottom.

Fig. B.14 shows the normalized values of the secondary parameters, (37) ($\dot{T}$ response), for the example wall. Since the tolerance criterion is the same, the amount of poles used in building up the response is the same as before for $\Delta t = 10$ [min] and $\Delta t = 60$ [min]. The φ_k parameter is the same in both Figures. It determines the exponential decay of the k-state with Δt.

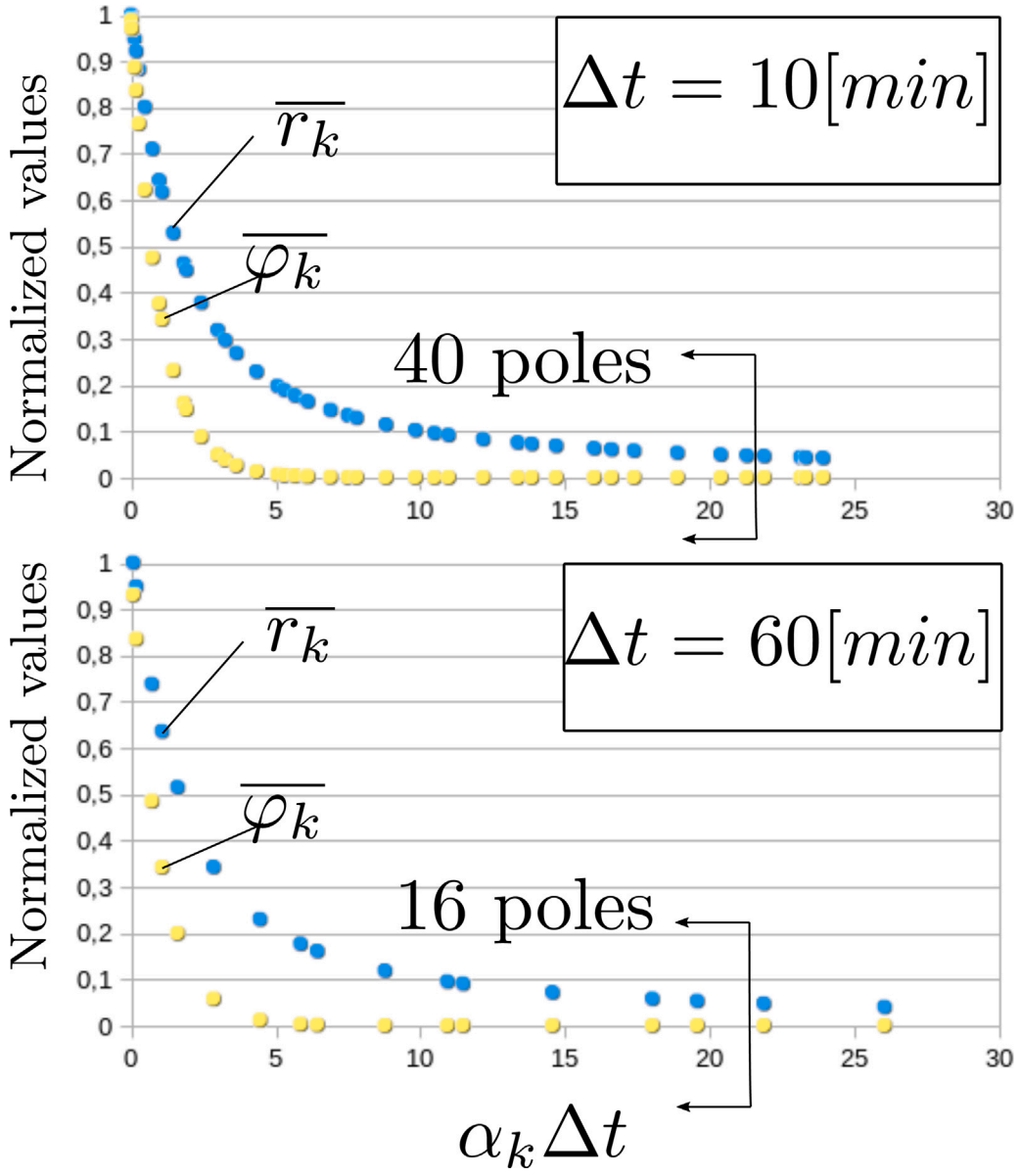

Fig. B.14. Secondary parameters for the $\dot{T}$ response, . (37), applied to the example wall and for two different elapsed times Δt, short at the top and long at the bottom.

B.3. Case 1: radom $\dot{q}$ values used in the example section of the SST method

See Table B.3.

Table B.3
Case 1: random conduction heat flux. Equals at both sides.

n	t [s]	$\dot{q}_{cond,0}$ [W/m^2]	$\dot{q}_{cond,1}$ [W/m^2]	Δt [s]
0	0	0.00	0.00	
1	1034	0.36	0.36	1034
2	2142	0.71	0.71	1108
3	4748	1.42	1.42	2606
4	6693	1.87	1.87	1945
5	9638	2.42	2.42	2945
6	12924	2.90	2.90	3286

(*continued on next page*)

Table B.3 (*continued*).

n	t [s]	$\dot{q}_{cond,0}$ [W/m^2]	$\dot{q}_{cond,1}$ [W/m^2]	Δt [s]
7	14291	3.07	3.07	1367
8	17514	3.39	3.39	3223
9	18646	3.49	3.49	1132
10	20454	3.62	3.62	1808
11	23517	3.81	3.81	3063
12	25597	3.92	3.92	2080
13	26340	3.95	3.95	743
14	29775	4.08	4.08	3435
15	33019	4.18	4.18	3244
16	34388	4.21	4.21	1369
17	35928	4.25	4.25	1540
18	38118	4.29	4.29	2190
19	39863	4.31	4.31	1745
20	41114	4.33	4.33	1251
21	41665	4.34	4.34	1251
22	42057	4.34	4.34	392
23	45090	4.38	4.38	3033
24	48759	4.41	4.41	3669
25	51282	4.44	4.44	2523
26	54693	4.45	4.45	3411
27	56655	4.46	4.46	1962
28	59434	4.47	4.47	2779
29	62167	4.47	4.47	2733
30	64550	4.48	4.48	2383
31	67960	4.48	4.48	3410
32	69013	4.48	4.48	1053
33	69562	4.48	4.48	549
34	71323	4.49	4.49	1761
35	73390	4.49	4.49	2067
36	77215	4.49	4.49	3825
37	77798	4.49	4.49	583
38	81058	4.49	4.49	3260
39	83238	4.49	4.49	2180
40	84582	4.49	4.49	1344
41	87150	4.50	4.50	2568

B.4. Case 2: radom $\dot{q}$ values used in the example section of the SST method

See Table B.4.

Table B.4
Case 2: random conduction heat flux. Equals at both sides.

n	t [s]	$\dot{q}_{cond,0}$ [W/m^2]	$\dot{q}_{cond,1}$ [W/m^2]	Δt [s]
0	0	0.00	0.00	
1	692	0.10	0.10	692
2	1038	0.15	0.15	346
3	1482	0.20	0.20	444
4	2160	0.30	0.30	678
5	2849	0.40	0.40	689
6	3550	0.45	0.45	701
7	4400	0.50	0.50	850
8	5045	0.55	0.55	645
9	5514	0.60	0.60	469
10	6336	0.65	0.65	822
11	6858	0.80	0.80	522
12	7544	1.20	1.20	686
13	8170	1.25	1.25	626
14	8791	1.26	1.26	621
15	9501	1.80	1.80	710
16	10159	2.00	2.00	658
17	10956	3.00	3.00	797
18	11580	4.00	4.00	624
19	12324	5.00	5.00	744
20	12836	5.50	5.50	512
21	13182	5.70	5.70	346
22	13563	5.80	5.80	381

(*continued on next page*)

Table B.4 (*continued*).

n	t [s]	$\dot{q}_{cond,0}$ [W/m^2]	$\dot{q}_{cond,1}$ [W/m^2]	Δt [s]
23	13959	5.90	5.90	396
24	14628	6.00	6.00	669
25	15201	6.10	6.10	573
26	15949	6.20	6.20	748
27	16807	6.30	6.30	858
28	17190	6.35	6.35	383
29	17733	6.40	6.40	543
30	18454	6.70	6.70	721
31	18924	6.70	6.70	470
32	19814	6.70	6.70	890
33	20561	1.00	1.00	747
34	21083	1.00	1.00	522
35	21525	1.00	1.00	442
36	22093	1.00	1.00	568
37	22434	1.00	1.00	341
38	23044	1.00	1.00	610
39	23835	1.00	1.00	791
40	24538	1.00	1.00	703
41	24870	1.00	1.00	332

References

[1] L. Mazzarella, M. Pasini, Conduction transfer function vs finite difference: Comparison in terms of accuracy, stability and computational time, in: Elsevier (Ed.), 6th International Building Physics Conference, Energy Procedia, 2015.

[2] Stephenson, Mitalas, Calculation of Heat Transfer Conduction Transfer Functions for Multi-Layer Slabs, ASHRAE, 1971.

[3] D.G. Stephenson, G.P. Mitalas, Cooling load calculations by thermal response factor method, Ashrae Trans. 73 (1967).

[4] I. Beausoleil-Morrison, in: Routledge (Ed.), Fundamentals of Building Performance Simulation, first ed., 2020, http://dx.doi.org/10.1201/9781003055273.

[5] K. Ernesto, M. Alexandre, Z.B. P., in: Elsevier, Academic Press (Eds.), Theory of Modeling and Simulation: Discrete Event and Iterative System Computational Foundations, Elsevier, Academic Press, 2019.

[6] Equation-based languages. a new paradigm for building energy modeling, simulation and optimization, Energy Build. 117 (2016) 290–300, http://dx.doi.org/10.1016/j.enbuild.2015.10.017.

[7] M. Wetter, K. Benne, A. Gautier, T. Nouidui, A. Ramle, A. Roth, in: Lawrence Berkeley National Laboratory (Ed.), Lifting the Garage Door on Spawn, an Open-Source Bemcontrols Engine, 2021, URL https://escholarship.org/uc/item/9c28b4qp.

[8] The gap between predicted and measured energy performance of buildings: A framework for investigation, Autom. Constr. 41 (2014) 40–49, http://dx.doi.org/10.1016/j.autcon.2014.02.009.

[9] S.J. Rees, Closing the performance gap through better building physics, Build. Serv. Eng. Res. Technol. 38 (2) (2017) 125–132, http://dx.doi.org/10.1177/0143624417693711.

[10] Benchmarking the practice of validation and uncertainty analysis of building energy models, Renew. Sustain. Energy Rev. 142 (2021) 110842, http://dx.doi.org/10.1016/j.rser.2021.110842.

[11] L. Mazzarella, R. Scoccia, P. Colombo, M. Motta, Improvement to EN ISO 52016-1:2017 hourly heat transfer through a wall assessment: the Italian national annex, Energy Build. 210 (2020) 109758, http://dx.doi.org/10.1016/j.enbuild.2020.109758, URL https://www.sciencedirect.com/science/article/pii/S0378778819328439.

[12] J.M. Pinazo Ojer, V.M. Soto Frances, E. Sarabia Escriva, L. Soto Frances, Thermal response factors to a 2nd order shaping function for the calculation of the 1D heat conduction in a multi-layered slab, Int. J. Heat Mass Transfer 88 (2015) 579–590, http://dx.doi.org/10.1016/j.ijheatmasstransfer.2015.04.110, URL https://www.sciencedirect.com/science/article/pii/S0017931015004810.

[13] V.-M. Soto-Francés, E.-J. Sarabia-Escrivá, J.-M. Pinazo-Ojer, P.-J. Martínez-Beltrán, Exploring the use of traditional heat transfer functions for energy simulation of buildings using discrete events and quantized state based integration, J. Build. Perform. Simul. 13 (3) (2020) 247–263, http://dx.doi.org/10.1080/19401493.2020.1723704, URL https://doi.org/10.1080/19401493.2020.1723704.

[14] T. Watanabe, A. Ozaki, Y. Urano, T. Hayashi, Y. Ryu, Practical methods for calculating unsteady-state heat conduction of multi-layer walls based on pulse transfer function, J. Archit. Plan. Environ. Eng. (Transactions of AIJ) 391 (1988) 8–19, http://dx.doi.org/10.3130/aijax.391.0_8.

[15] V.M. Soto Frances, E.J. Sarabia Escriva, J.M. Pinazo Ojer, Discrete event heat transfer simulation of a room, Int. J. Therm. Sci. 75 (2014) 105–115, http://dx.doi.org/10.1016/j.ijthermalsci.2013.07.024, URL https://www.sciencedirect.com/science/article/pii/S1290072913001889.

[16] D.C. Hittle, Calculating Building Heating and Cooling Loads Using the Frequency Response of Multilayered Slabs, University of Illinois, Urbana, IL., 1979, URL https://apps.dtic.mil/sti/citations/ADA097597.

[17] D.C. Hittle, R. Bishop, An improved root-finding procedure for use in calculating transient heat flow through multilayered slabs, Int. J. Heat Mass Transfer 26 (11) (1983) 1685–1693, http://dx.doi.org/10.1016/S0017-9310(83)80089-1, URL https://www.sciencedirect.com/science/article/pii/S0017931083800891.

[18] G. Migoni, E. Kofman, F. Cellier, Quantization-based new integration methods for stiff ODEs, Simul.: Trans. Soc. Model. Simul. Int. 88 (4) (2012) 387–407, URL.